

Conformations of dendrimers in dilute solution

Edward G. Timoshenko*

Theory and Computation Group, Centre for Synthesis and Chemical Biology, Conway Institute for Biomolecular and Biomedical Research, Department of Chemistry, University College Dublin, Belfield, Dublin 4, Ireland

Yuri A. Kuznetsov

Centre for High Performance Computing Applications, University College Dublin, Belfield, Dublin 4, Ireland

Ronan Connolly

Theory and Computation Group, Department of Chemistry, University College Dublin, Belfield, Dublin 4, Ireland
(February 1, 2008)

Conformations of isolated homo- dendrimers of $G = 1 - 7$ generations with $D = 1 - 6$ spacers have been studied in the good and poor solvents, as well as across the coil-to-globule transition, by means of a version of the Gaussian self-consistent (GSC) method and Monte Carlo (MC) simulation in continuous space based on the same coarse-grained model. The latter includes harmonic springs between connected monomers and the pair-wise Lennard-Jones potential with a hard core repulsion. The scaling law for the dendrimer size, the degrees of bond stretching and steric congestion, as well as the radial density, static structure factor, and asphericity have been analysed. It is also confirmed that while smaller dendrimers have a dense core, larger ones develop a hollow domain at some separation from the centre.

PACS numbers: 36.20.-r, 36.20.Ey, 61.25.Hq

I. INTRODUCTION

Dendrimers represent a class of well defined hyper-branched macromolecules¹ which can be synthesised via a sequence of carefully controlled repetitive reactions producing regular structures². There are high aspirations^{3,4} of chemists and physicists regarding applications of such novel polymers as advanced materials for medicinal⁵ uses, superior catalysts^{6,7}, and drug delivery vehicles⁸, to mention just a few. Importantly for such applications, dendrimers are quite flexible molecules, which have a well accessible interior part as well as a large exterior surface. Furthermore, dendrimers can controllably change their size and density distribution under the influence of external conditions. Some of the potential applications of dendrimers moreover require a hollow interior, which could be used for accommodating guest molecules⁹. In addition, spacers, charges, and distinct types of monomer units should allow one to further fine tune particular behaviour of dendrimers.

Although the ideal model of dendrimers with the harmonic springs or random walks can be solved analytically¹⁰, such results are of a limited value since the excluded volume interactions are of paramount importance for dendrimers¹¹. However, including these in order to describe the range of the coil-to-globule transition in sufficient detail is a considerable challenge even for the homo- dendrimer. This problem has attracted a number of researchers yielding a significant body of theoretical and computational work in recent years, with some experimental results¹² available to assist them.

De Gennes and Hervet¹³ have performed a seminal calculation using a version of the Edwards' self-consistent field method upon an assumption that an onion-like layered distribution of the dendrimer generations applies. They have predicted a density minimum at the core of the dendrimer and the scaling law for the radius of gyration, $R_g \sim N^{1/5}$, where N is the total number of monomers, both of which henceforth have been debated. Later on Boris and Rubinstein¹⁴ have proposed a more complicated self-consistent mean-field and related Flory-type theories. They have found that the density is monotonically decreasing with a maximum at the core. However, such a theory does not contain spatial correlations and thus may have considerable limitations in predicting the internal structure of dendrimers.

*Corresponding author. Web: <http://darkstar.ucd.ie>; E-mail: Edward.Timoshenko@ucd.ie

A version of the Gaussian variational theory¹⁵, which relies on a somewhat problematic¹⁶ virial representation of the excluded volume interactions^{17,18}, has been used by Ganazzoli *et al* for describing the size, shape and intrinsic viscosity of dendrimers in a good solvent¹⁹. Based on this approach the dynamic properties such as the relaxation times spectrum, dynamic structure factor and the viscoelastic moduli²⁰, as well as the inter-chain theta-temperature²¹ have been also investigated. Unfortunately, constraints of the numerical procedure employed limited such studies to dendrimers with $D = 1, 2$ spacers only.

A number of simulation studies using either Molecular Dynamics (MD) or Monte Carlo (MC), both on and off-lattice, whether atomistically detailed or coarse-grained, have been also performed. Naylor *et al*²² have discussed the MD simulation of PAMAM (poly(amido-amine)) dendrimers. This study, albeit generally interesting, could cover a timescale of hundreds of picoseconds only. Later Lescanec and Muthukumar²³ have proposed a kinetic growth model in a 3-d off-lattice MC. They have reported the highest density at the core and have also found that the terminal monomers can traverse the dendrimer. Their approach, however, was in essence a non-equilibrium one as sufficient equilibration was not been allowed. This may explain a rather small reported value of the swelling exponent $\nu \simeq 0.22$ in the proposed scaling law $R_g \sim N^\nu D^{1/2}$ for the good solvent. Next, Mansfield and Klushin²⁴ have performed a MC simulation on a diamond lattice with $D = 7$ spacers modelled as self-avoiding walks. Their paper has managed to overcome some of the previous limitations and it contained some important insights. Nevertheless, the D dependence has not been investigated there. Furthermore, a possibility of lattice artefacts for the restricted branch points may raise some doubt in the more refined features of their predictions. Chen and Cui²⁵ have performed off-lattice MC simulations for a good solvent in a model with freely rotating bonds. They have also attempted to fit the radius of gyration as $R_g \sim D^\nu 2^{(2\nu-1)G} G^{1-\nu}$, i.e. in terms of both D and the number of generations G . While the value of ν has been related to the inverse fractal dimension of the open/ring chain, just as in Ref. 26 containing the renormalisation group calculation by Biswas and Cherayil, the meaning of the G -dependent part of the scaling law lacked such clarity.

Further MD simulation by Murat and Grest²⁷ has relied on a coarse-grained model with the Lennard-Jones non-bonded and the FENE bonded interactions employing a white noise for the solvent and temperature effects. This simulation involved sufficient equilibration times and has yielded a number of interesting results. For instance, the dendrimer size at a fixed number of spacers D in a good solvent was found to scale as $R_g \sim N^\nu$ with the value of the exponent ν surprisingly close to $1/3$. Interestingly, the indication about a hollow domain inside the dendrimer, which has been first noted in Ref. 24, has been reiterated and further elaborated by performing the partial densities analysis over generations. These authors have also looked at the dendrimer contraction on changing the solvent quality from good to poor. They have concluded that the law $R_g \sim N^{1/3}$ (at fixed D) applies for the more compact globular dendrimer, which seemed reasonable from the point of view of the space filling argument.

Despite this considerable progress, understanding of the homo- dendrimers is not as yet fully satisfactory. First, a reasonably large span of spacer and generation numbers under variable solvent conditions has until now been hard to study. Second, it was difficult to achieve both a reliable equilibration and a good averaging statistics afterwards at the level of affordable computational times. Clearly though, these requirements must be met at the same time in order to be able to extract reliable scaling predictions and to make firm conclusions on the intricacies of the internal structure of dendrimers. Moreover, not only the good, but the theta- and poor solvents, as well as the thermodynamics of the coil-to-globule, are of interest. Perhaps, particular deficiencies of the techniques employed, an insufficient accuracy, and a limited range of systems may explain some of the discrepancies which remained between the results of different approaches. Therefore, we believe that it would be important to revisit the problem.

Here we shall try to re-examine the fundamentals of dendrimers in a broader context of their overall conformational behaviour as a function of the solvent quality. On the one hand, this may help to resolve some of the remaining controversy in the concrete predictions. On the other hand, it may shed some new light on the problem thanks to studying the observables which hitherto have not been investigated and to performing a type of analysis which is more novel. Last but not least, one may hope to improve the statistics and to study a broader range of dendrimers by using a well optimised MC code²⁸⁻³⁰ on faster modern computers³¹.

Our recent progress³² on extending the Gaussian self-consistent (GSC) method may offer some advantages and permit comparisons to be made with the simulation data. The improved technique avoids the use of a virial expansion, but instead operates directly with a given Hamiltonian involving any pair-wise bonded and non-bonded interactions, just as in direct simulations. Ref. 32 deals with all the technical details and it contains a comprehensive comparison with the MC data performed for open, ring and star homopolymers with variable flexibility in a good and poor solvents. The method appears to be relatively accurate for a number of observables and its limitations are well understood. Because the new GSC technique is computationally very fast and since it directly yields the equilibrium averages for the observables of interest, it will allow us to consider a larger range of system sizes and a broader region of solvent conditions than with the equivalent MC simulation.

II. MODEL AND NOTATIONS

The current coarse-grained homo-dendrimer model is based on the following Hamiltonian (energy functional)^{30,29,33} in terms of the monomer coordinates, \mathbf{X}_i :

$$\frac{H}{k_B T} = \frac{1}{2\ell^2} \sum_{i \sim j} \kappa_{ij} (\mathbf{X}_i - \mathbf{X}_j)^2 + \frac{1}{2} \sum_{ij, i \neq j} U^{(lj)}(|\mathbf{X}_i - \mathbf{X}_j|). \quad (1)$$

Here the first term represents the connectivity of the dendrimer with harmonic springs of strength κ_{ij} introduced between any pair of connected monomers (which is denoted by $i \sim j$). The second term represents pair-wise non-bonded, specifically van der Waals interactions between monomers. We shall adopt the Lennard-Jones form of the potential,

$$U^{(lj)}(r) = \begin{cases} +\infty, & r < d^{(0)} \\ U^{(0)} \left(\left(\frac{d^{(0)}}{r} \right)^{12} - \left(\frac{d^{(0)}}{r} \right)^6 \right), & r > d^{(0)} \end{cases}, \quad (2)$$

with hard core part and the monomer diameter $d^{(0)}$, where $U^{(0)}$ is the dimensionless strength of the interaction.

It is important to introduce convenient notations. Let us consider a dendrimer of G generations, each of which consists of D spacers, with F_0 functional core (corresponding to the generation $g = -1$) and F functional other branch points (see Fig. 1). Thus, if $D = a$ and $G = b$ we shall briefly denote such a dendrimer as DaGb as in Refs. 19,20. Then the total number of monomers will be,

$$N = 1 + F_0 D \frac{(F - 1)^{G+1} - 1}{F - 2}. \quad (3)$$

Note that below we shall consider results for a particular example of tri-functional branching $F = F_0 = 3$. It is convenient to represent monomer indices via triads $i = (g, d, \varphi_g)$, where $g = 0, 1, \dots, G$ is the generation index, $d = 0, 1, \dots, D - 1$ is the spacer index, and $\varphi_g = 0, 1, \dots, F_0(F - 1)^g - 1$ is the angular in-generation index. It is also useful to define the shell radial index via $\rho = Dg + d + 1$, and hence instead of the triad, one can use the ‘polar coordinates’ index notation $i = (\rho, \varphi_g)$. Both of these will be used interchangeably henceforth.

III. TECHNIQUES

A. Monte Carlo technique

We use the Monte Carlo (MC) technique with the standard Metropolis algorithm³⁴ and local monomer moves, based upon the implementation described by us in Refs. 28,30. The position of a randomly picked monomer in the spherical coordinates is displaced by $\Delta r = \delta r_1$, $\Delta \theta = \pi \theta_1$, $\Delta \phi = 2\pi \phi_1$ where (r_1, θ_1, ϕ_1) is a triple of independent standard uniform deviates and δ is an additional parameter of the MC scheme characterising the timescale involved in the Monte Carlo sweep (MCS), the latter being defined as N attempted MC steps. The Metropolis check, $\Delta E \leq -k_B T \ln r_1$, where r_1 is yet another standard uniform deviate, is then used as a criterion for accepting trial new conformations. As a result, the ensemble of independent initial conformations would converge to the Gibbs equilibrium distribution with increasing number of sweeps. Initial conformations of dendrimers were taken as planar and rather overstretched ones (akin to the schematic representation in Fig. 1), but then they were subjected to extensive equilibration for a required time before any simulation was commenced.

To ensure good equilibration, the behaviour of global observables such as the energy and radius of gyration was monitored. Upon reaching equilibrium these cease to have a global drift and start exhibiting characteristic fluctuating behaviour around well defined mean values. Then, depending on the dendrimer size, about $Q = 2 \cdot 10^4$ of statistical measurements have been performed, typically separated by about $40N^2$ of attempted Monte Carlo steps to ensure statistical independence of sampling. The mean value and error of sampling of an observable A are then given by the mean $\langle A \rangle = (1/Q) \sum_{\gamma}^Q A_{\gamma}$ and by $\pm \sqrt{(\Delta A)^2 / Q}$ respectively.

B. The Gaussian Self-Consistent method

The main objects in the GSC method are the mean-squared distances between monomers,

$$\mathcal{D}_{ij}(t) \equiv \frac{1}{3} \left\langle (\mathbf{X}_i(t) - \mathbf{X}_j(t))^2 \right\rangle. \quad (4)$$

The GSC method is based on replacing the stochastic ensemble for \mathbf{X}_i with the exact Hamiltonian in the Langevin equation of motion onto the trial ensemble $\mathbf{X}_i^{(0)}(t)$ with a trial Hamiltonian $H^{(0)}(t)$, which is a generic quadratic form with matrix coefficients called the time-dependent effective potentials,

$$H^{(0)}[\mathbf{X}(t)] = \frac{1}{2} \sum_{ij} V_{ij}(t) \mathbf{X}_i(t) \mathbf{X}_j(t). \quad (5)$$

Then one requires that the inter-monomer correlations satisfy the condition,

$$\langle \mathbf{X}_i(t) \mathbf{X}_j(t) \rangle_0 = \langle \mathbf{X}_i^{(0)}(t) \mathbf{X}_j^{(0)}(t) \rangle_0, \quad (6)$$

which means that the trial ensemble well approximates the exact one. This yields the self-consistent equations²⁹, which in the absence of the hydrodynamic interactions are,

$$\frac{\zeta_b}{2} \frac{d}{dt} \mathcal{D}_{ij}(t) = -\frac{2}{3} \sum_k (\mathcal{D}_{ik}(t) - \mathcal{D}_{jk}(t)) \left(\frac{\partial \mathcal{A}[\mathcal{D}(t)]}{\partial \mathcal{D}_{ik}(t)} - \frac{\partial \mathcal{A}[\mathcal{D}(t)]}{\partial \mathcal{D}_{jk}(t)} \right). \quad (7)$$

Here ζ_b is the friction coefficient of a monomer and the instantaneous free energy has the same functional expression via the instantaneous $\mathcal{D}_{ij}(t)$ as it has at equilibrium.

The expression for the free energy, $\mathcal{A} \equiv \mathcal{E}^{(tot)} - T\mathcal{S}$ has been given in Ref. 32. We would not like to reproduce that expression here as it is somewhat cumbersome. However, it should be mentioned that the total mean energy includes the energy of the bonded and non-bonded interactions \mathcal{E} as well as the hard-core contribution as follows, $\mathcal{E}^{(tot)} = \mathcal{E} + \mathcal{A}^{(hs)}$. The second term is given by the generalised Carnahan-Starling term^{35,32},

$$\frac{\mathcal{A}^{(hs)}}{k_B T} = \sum_i \frac{\eta_i(4 - 3\eta_i)}{(1 - \eta_i)^2}, \quad \eta_i = \sum_{j \neq i} F^{(\eta)} \left[\frac{\sqrt{\mathcal{D}_{ij}}}{d^{(0)}} \right], \quad (8)$$

$$F^{(\eta)}[y] = \frac{y \operatorname{erf}\left(\frac{1}{y\sqrt{2}}\right) - \sqrt{2/\pi} \exp\left(-\frac{1}{2y^2}\right)}{8y}, \quad (9)$$

where η_i is known as the packing coefficient of the monomer i , which would have an important role below.

The stationary limit of the GSC Eqs. (7) produces the equations for the minimum of the free energy, which are the same as those derived from the Gibbs-Bogoliubov variational principle. Although here we shall only be concerned with the equilibrium, the numerical solution of Eq. (7), applied until the stationary limit is reached, presents one of the most efficient techniques for finding the global free energy minimum. This, based on the fifth order adaptive step Runge-Kutta integrator¹⁶, is used for obtaining the results from the GSC technique.

It is also important to map out all equivalent pairs of the matrix \mathcal{D}_{ij} , which is discussed in Appendix A based on the concept of the topological tree, so that only $C_{ind}^{(2)} = (G+1)(D/2)(D(G^2/3 + (13/6)G + 2) + 2 + G/2)$ independent elements out of total $C_{tot} = N(N-1)/2$ remain in it due to the kinematic symmetries of the dendrimer. It is interesting to remark, more generally, that exactly the same symmetries will exist for a hetero-dendrimer as long as the monomers at each shell index ρ are identical to each other.

The kinematic symmetries for the matrix \mathcal{D}_{ij} also yield analogous symmetries for the matrix V_{ij} . Thus, the computational expenses per step in our calculations are of order $t_c \sim N C_{ind}^{(2)}$, where $C_{ind}^{(2)} \sim D^2 G^3/6$ is the total number of independent elements in the \mathcal{D}_{ij} matrix (see Eq. (A1)). These symmetries significantly reduce the computational times compared to the equivalent system in the MC method, where such symmetries only appear in the observables after averaging over the statistical ensemble. For comparison, the computational expenses per step in MC are of order $t_c \sim N \Delta t S$, where $\Delta t \sim N^2$ is the number of MC steps needed to ensure good statistical independence between measurements, and S is the number of measurements needed for sampling of observables. Typical values of S should be of order of $10^4 - 10^5$ for good accuracy³⁰. For example, for D3G5 dendrimer (consisting of $N = 568$ units) in the good solvent, $U^{(0)} = 1$, the GSC method takes about 22 minutes³¹ to reach equilibrium and produce its data, whereas the MC manages to make only 100 measurements of observables per hour after required equilibration. Thus, the GSC is about 10^3 times faster than the MC for producing the same results here.

IV. RESULTS

We shall restrict ourselves to springs of equal strength, $\kappa_{ij} = 1$, and choose the hard sphere diameter equal to the statistical length, $d^{(0)} = \ell$, in Eq. (1) as in Ref. 30. Moreover, henceforth we shall use the mean energy \mathcal{E} expressed in units of $k_B T$ and the mean-squared distances \mathcal{D}_{ij} and mean-squared radius of gyration, $3\mathcal{R}_g^2$, expressed in units of ℓ^2 .

In our figures below we shall present data from MC simulation via thick lines and empty circles, whereas data from GSC theory via thin lines and small filled circles. In this work we have analysed the following dendrimer sizes: $G = 1 - 7$ for $D = 1 - 3$ and $G = 1 - 6$ for $D = 4 - 6$.

A. Good solvent

We shall start by examining the dendrimer overall size and structure in the good athermal solvent, $U^{(0)} = 0$.

The mean-squared radii of gyration $3\mathcal{R}_g^2$ of dendrimers with varying number of spacers D vs the number of generations G are depicted in Fig. 2. Clearly, $3\mathcal{R}_g^2$ increases with both D and G , but in a rather different manner, which will be discussed in full detail below in Subsec. IV C. Corresponding MC and GSC curves follow each other quite closely, but the GSC theory increasingly overestimates the dendrimer size with increasing D and G , in a manner similar to our discussion in Ref. 32.

As G increases, dendrimers become more spherical, which is illustrated via the average normalised ‘axes of inertia’ $\lambda^{(a)}$ defined by Eqs. (9,10) in Ref. 30. These converge towards a perfect sphere limit, $\lambda^{(a)} = 1/3$, as G grows in Fig. 3. Interestingly, these quantities seem to be practically independent of the number of spacers D , which is illustrated by using circles ($D = 4$) and lines ($D = 2$) in the figure.

Typical snapshots of dendrimers D3G3 and D3G7 in Figs. 4 from MC simulation do confirm the observation that dendrimers become more spherical as G increases. Generally, a fairly large dendrimer tends to fill in the available space quite effectively and relatively uniformly, although some local dilutions and accumulations remain. The size of the dendrimer is well defined with very few branches outstretching beyond it.

The shape of the static structure factor (SSF) in the Kratky representation in Fig. 5 for small G is reminiscent of that of a ring, or a star with few arms (see Figs. 9,10 in Ref. 30), but tends more to that of a globule with increasing number of generations. Even though the tail of the plot still increases with \hat{p} , it develops a characteristic oscillating behaviour. This is consistent with the trends in $\lambda^{(a)}$ above, particularly so since the D -dependence is almost unnoticeable in \hat{S} as well.

The total and partial densities,

$$g_g^{(1)}(r) \equiv \sum_{i \in g} \langle \delta(\mathbf{r}_i - \mathbf{r}_{cm} - \mathbf{r}) \rangle, \quad 4\pi \int_0^\infty r^2 dr g_g^{(1)}(r) = N_g = F_0 D (F - 1)^g. \quad (10)$$

of the dendrimers in Figs. 6 allow one to understand the monomer distributions in more detail. In a relatively small- G dendrimer (Fig. a) the total density monotonically decreases with the separation from the centre-of-mass \mathbf{r}_{cm} . The highest density at the origin also occurs for the partial density of inner generations, and it follows a similar pattern. Remarkably, the terminal generation density is rather delocalised spreading evenly from the outer boundary towards the very centre of the dendrimer. This can only be rationalised by allowing a possibility of the ends re-entering the dendrimer and reaching far inside, although the density of the terminal generation exceeds that of the others somewhat near the very edge of the dendrimer.

These features are further complicated for dendrimers of a greater number of generations, typically for $G > 5$, at least in the considered cases of $D = 2, 4$. While the behaviour of the terminal generation density remains very similar in Fig 6b, the density of non-terminal generations, and hence the total density, develop a well noticeable dip at certain separation. This indicates that larger- G dendrimers have the lowest density domain fairly close to the centre, but not at the centre itself, which always has the highest density of all. We may note here also that while the core monomer coordinate does differ from that of the centre-of-mass somewhat, they are quite close to each other in a large- G dendrimer. Thus, this most hollow domain is not located where the core monomer is and its separation from the core steadily increases with G . Clearly, from Fig 6b one can see that the increase of the total density at the origin comes entirely from the density of the innermost generations. However, the core domain is at its most dense in a small- G dendrimer and it becomes less dense for larger dendrimers (in terms of both G and D actually) as can be seen by comparing the values of $g^{(1)}(r = 0)$ in Figs. 6a and b. This ‘entropic pull’ effect is due to an increased entropy thanks to extra branches attached to a larger dendrimer, leading to a higher stretching of the springs near the core with larger G .

Indeed, in Figs. 7,8,9 we depict the mean-squared distances between nearest neighbours along a branch vs the shell index ρ . This is perhaps the best way to characterise such stretching. While the main bodies of Figs. 7,8 present the data from MC simulation, the insets exhibit the same results obtained from the GSC theory. Clearly, the concrete numbers for $\mathcal{D}_{(\rho-1,0)}(\rho,0)$ are somewhat overestimated by the GSC theory compared to the MC data³², especially for small ρ in relatively large- G dendrimers. Nevertheless, the particular patterns and overall shapes of the MC and GSC plots are rather similar.

As can be seen from Fig. 7, for small dendrimers D2G1-3, the spring from the core to the first monomer is stretched most, from the first to the second one is less, and so on, with the function $\mathcal{D}_{(\rho-1,0)}(\rho,0)$ decreasing monotonically. However, for dendrimers with $G > 3$ the function develops a characteristic descending step-like behaviour: the spring stretching within the same generation is about the same, but it has a dramatic drop when passing the branch point to the next generation. In all cases though, the bonds coming from the core are stretched most, with this feature becoming stronger for larger G , whereas the terminal bonds are the least stretched of all, with their length being nearly G -independent. The step-like behaviour can be easily interpreted by remarking that the number of springs doubles at any branch point. Hence the total unfavourable energy change due to a given magnitude of bonds stretching would be more significant near the edges than closer to the core. Note also that the step-like dependence vanishes for the terminal generation.

Plots in Fig. 8 for $D = 4$ spacers show that the stretching near the core increases significantly with G here as well. One can also see that the intra-generational steps develop a non-monotonic behaviour. Bonds within a non-terminal generation first become shorter with increasing index d until about $D/2$, then grow longer again when approaching the next branch point. This U-pattern occurs because there is more steric congestion near the branch points than in the middle of generations. The terminal generation is the least stretched here as for $D = 2$ and it has a similar monotonically diving behaviour ending up at a G independent stretching value. Similar plots for dendrimers with $D = 6$ spacers in Fig. 9 obtained from the GSC theory show the U-pattern becomes more pronounced as D increases.

Finally, to address the issue of steric congestion we shall analyse the behaviour of the monomer packing coefficient η_i defined by Eqs. (8,9). This quantity shows the volume fraction occupied by all other monomers around a given monomer number i , with the limit $\eta_i \rightarrow 1$ corresponding to the fully packed situation according to Eq. (8).

In Figs. 10,11 the packing coefficients vs the shell index ρ along a branch are shown for different dendrimers with $G = 6$ and $D = 3$ respectively. For the former case it is convenient to normalise the horizontal axis as ρ/D so that branch points occur at integer values $0, \dots, G$ with $G + 1$ corresponding to the terminus. In Fig. 10 different curves correspond to different numbers of spacers D . The curve for $D = 1$ gives a general outline of η_ρ behaviour. The packing coefficient, and hence congestion, first increases, reaches a maximum and then rapidly decreases towards the termini, which are less crowded than the core domain. A larger number of spacers D leads to an U-pattern behaviour for $g < G$ and a rapid dive for the terminal generation, similar to our discussion of Fig. 9. Again, the middle of generations, where η_ρ has smooth minima, has a lower steric congestion since the monomers have only two nearest neighbours along the chain there compared to three for branch points, where η_ρ has sharp maxima. As for the terminus, it has a single nearest chain neighbour only, resulting in a pronounced minimum of η_ρ .

In Fig. 11 we likewise present the packing coefficients for dendrimers with increasing number of generations G and the fixed number of spacers $D = 3$. The general behaviour of η_ρ is similar here. For small $G < 5$ the function η_ρ oscillates around a constant, dropping down dramatically on the terminal generation. However, in larger dendrimers, $G \geq 5$, the function η_ρ starts from much lower values for small ρ and then increases overall up to penultimate generations, dropping down for the terminal g . Such behaviour is consistent with a lower density domain near the core seen via the spatial density distribution in Fig. 6b. For the D3G7 dendrimer, the lowest packing coefficient value occurs at around the middle of the $g = 0$ generation (monomers 1,2,3 in diagram Fig. 1, which are buried deep inside the dendrimer as in Fig. 4b). Note also that here we have $\eta_{D(G+1)} > \eta_0$, indicating the onset of overcrowding in the terminal generation, which would become very severe for larger G . Overall, the packing coefficient typically changes nearly twice in its value for relatively large D and $G = 6$, whereas the range of change in η_ρ increases further with increasing G .

Limited simulations with a smaller monomer diameter $d^{(0)} = 0.3\ell$ have been also performed and similar results have been obtained. Dendrimers with such reduced repulsions are more compact and, clearly, as $d^{(0)}$ is decreased further they change in a cross-over manner towards the behaviour of the ideal dendrimers.

B. Coil-to-globule transition and poor solvent

Now we shall bring our attention to the coil-to-globule transition. Upon increasing Lennard-Jones attraction $U^{(0)}$ the dendrimer contracts and the mean-squared radius of gyration decreases as shown in Fig. 12a. The magnitude of this change is quite significant, being over 20 times for D6G5 dendrimer. As our plot is drawn in a single logarithmic

scale one can see that the region of maximal relative change in value of $3\mathcal{R}_g^2$ occurs at around $U^{(0)} \simeq 2.5$, with the change being more pronounced in larger dendrimers. Clearly, from this plot and from Fig. 12b, which depicts the derivative of the specific mean energy, one can conclude that the transition is continuous (second-order like).

The quantity $d(\mathcal{E}/N)/dU^{(0)}$ changes from one asymptotic behaviour at small $U^{(0)}$ to another at large arguments, reaching eventually a constant value corresponding to the maximal packing. The maximal change in this quantity occurs at $U_{\mathcal{E}'}^{(0)} \simeq 2.5$, which may be viewed as a reasonable practical definition of the transition point³². As the transition is continuous it has a finite width and hence any such definition is somewhat arbitrary. However, as N increases the transition narrows and becomes sharper. It would be easy to consider the point of vanishing of the non-bonded part of the second virial coefficient (binary integral), $u_{LJ}^{(2)} \equiv (1/2) \int d\mathbf{r} (1 - \exp(-U^{(lj)}(|\mathbf{r}|)))$, which occurs at about $U_{LJ}^{(0)} \simeq 1.386$. Unfortunately, such a definition of the theta-point is unacceptable as it produces a result which does not depend on the polymer connectivity or size. Instead, one has to consider the total $u^{(2)}$ with the full account of the bonded and non-bonded interactions. This, however, is technically quite complicated as the Mayer-Ursell expansion is not easy to apply to dendrimers with both types of interactions involved. Thus, we shall use $U_{\mathcal{E}'}^{(0)}$ as a convenient numerical definition of a point which becomes close to the exact theta-point for sufficiently large N .

In Tab. I we report the values of $U_{\mathcal{E}'}^{(0)}$ for dendrimers with varied D and G . Clearly, either increased number of generations or spacers, and hence increased N , would lead to a lower value of $U_{\mathcal{E}'}^{(0)}$ (larger temperature $T_{\mathcal{E}'}$) of the transition. Indeed, the point $U_{\mathcal{E}'}^{(0)}$ corresponds to the compensation of the positive conformational entropy $\mathcal{S}^{(gau)}$ with the negative two-body $\mathcal{E}^{(lj)}$ energy growing as N^2 and much faster than $\mathcal{S}^{(gau)}$ in N , so that smaller $U_{\mathcal{E}'}^{(0)}$ would suffice for the compensation. More non-trivially though, if we compare, for example, D3G6 and D6G5 dendrimers, both having about the same N , the larger D system would have a lower $U_{\mathcal{E}'}^{(0)}$ (larger temperature $T_{\mathcal{E}'}$).

For linear or ring polymers one can alternatively define the theta-point of the current model by finding a value of $U^{(0)}$ at which the radius of gyration of the system matches that of the corresponding ideal system ($d^{(0)} = 0$). In Tab. I such values $U_{\mathcal{R}}^{(0)}$ are presented in parentheses. Clearly though, this definition is inappropriate for dendrimers as $U_{\mathcal{R}}^{(0)}$ shifts deep into the globular area for dendrimers with sufficiently large G .

The region beyond $U_{\mathcal{E}'}^{(0)}$ corresponds to a globular conformation of the dendrimers, to discussion of which we shall now turn. In Fig. 13 we display the mean-squared radii of gyration for dendrimers with different number of spacers D vs the number of generations G . The solid lines correspond to the globule with $U^{(0)} = 7$, that is, well beyond the transition region, whereas the dashed lines correspond to similar ideal dendrimers ($d^{(0)} = 0$ and $U^{(0)} = 0$). These grow with D at a fixed G , and vice versa in both cases. Interestingly, while the globule is more compact than the corresponding ideal dendrimer at relatively small G , for D1G>6 this trend reverses. This is due to a significant role of the repulsive part of the non-bonded potential in dendrimers with excluded volume interactions and it shows a limited relevance of the model of ideal dendrimers when applied to the coil-to-globule transition. In fact, the scaling behaviour at the transition point differs from that of the ideal dendrimer unlike in the simpler cases of open or ring polymers. Such issues will be examined by us further in Subsec. IV C.

Next, we shall compare the mean-squared distances between nearest neighbours along a branch vs the shell index ρ for the globule in Fig. 14 to that in the good solvent in Fig. 9. The function $\mathcal{D}_{(\rho-1,0)}(\rho,0)$ here has a similar U-pattern inside each generation, a dive at the terminal generation, and it increases as G is increased, just as before. However, the descending stairway behaviour seen for the good solvent is no longer present now even for large G , and the function oscillates around a constant value. Thus, the bond stretching near the core is reduced, and apart from the intra-generational variation and the special role of the termini, the globular dendrimers are fairly evenly stretched as well as have uniform density (see inset in Fig. 6a). Note also that the maxima occur at pairs of subsequent chain indices ρ . This means that the mean-squared distances from the pre-branch monomer to the branch point are almost the same as from the branch point to the post-branch one, which indicates similarity in overall bond stretching with increasing ρ and hence an approximate equivalence of all branch points in the globule. Therefore, the connectivity structure of the dendrimer is less significant and more locally manifested in the globular state.

Similar conclusions can be made also from the behaviour of the monomer packing coefficient for globular dendrimers in Fig. 15. Again, η_ρ only depends periodically on the spacer index d , being nearly identical for all generations but the terminal one. The peaks occur at the branch points and the termini have the lowest packing coefficient of all just as for the good solvent in Fig. 11. Note, however, that the actual magnitudes of η_ρ are much larger for the globule than for the good solvent and approach 1/2. Moreover, the mean value of η_ρ in the globule steadily increases with N and there is no hollow domain in the globular conformation even for $G > 5$. Indeed, the total density $g^{(1)}(r)$ of a globule dendrimer shown in the insets of Figs. 6a,b is practically uniform and rather localised within the size of the globule, thus having higher values than for the good solvent. Remarkably, the terminal generations still can traverse the dendrimer even in such a dense state.

C. Scaling relations

First, one can fit the mean-squared radii of gyration at a fixed number of generations G in terms of N expressed via D by Eq. (3) as,

$$\text{Good solvent: } \sqrt{3\mathcal{R}_g^2} = a_G N^{\nu_G}, \quad (11)$$

$$\text{Theta-solvent: } \sqrt{3\mathcal{R}_g^2} = a_G N^{\nu_G}, \quad (12)$$

$$\text{Poor solvent: } \sqrt{3\mathcal{R}_g^2} = A_G N^{\nu_G}. \quad (13)$$

The values of the exponent ν_G obtained from fitting of the data are presented in Tab. II,

$$\text{MC: } \nu_G \simeq 0.58 \pm 0.02, \quad (14)$$

$$\text{GSC: } \nu_G \simeq 0.62 \pm 0.01. \quad (15)$$

Note that ν_G here practically coincides with the inverse fractal dimension of an open repulsive chain. Thus, we can interpret ν_G as the Flory swelling exponent, the value of which for large N is more accurately known from the renormalisation group calculation, namely $\nu_F = 0.588 \pm 0.001$. As discussed in Ref. 32 the GSC theory overestimates the Flory swelling exponent by about 0.04 as compared to the MC data for this range of finite polymer sizes. This is consistent with the amount by which the GSC values for ν_G exceed those of the MC simulation.

At the same time, the prefactor a_G does not obey a power law in G , but it can be fitted well via the following expression,

$$\text{GSC: } a_G = (0.74 \pm 0.01) 2^{-\frac{G+1}{4.07 \pm 0.1}}, \quad \text{MC: } a_G = (0.9 \pm 0.03) 2^{-\frac{G+1}{3.9 \pm 0.2}}. \quad (16)$$

Or by using Eq. (3) again, we can express this for the good solvent via,

$$\sqrt{3\mathcal{R}_g^2} \sim \left(\frac{3D}{N}\right)^{1/4} N^{\nu_F} \sim D^{1/4} N^{\nu_F-1/4}, \quad (17)$$

$$\sqrt{3\mathcal{R}_g^2} \sim D^{\nu_G} (F-1)^{\nu_D (G+1)}, \quad \nu_D \approx \nu_G - \frac{1}{4}. \quad (18)$$

Indeed, as can be seen from Tab. III, the resulting exponent $\nu_D \simeq 0.37 \pm 0.01$ in the GSC method, whereas from MC the resulting exponent value is $\nu_D \simeq 0.335 \pm 0.008 \gtrsim 1/3$. These notations for the exponents ν_G , ν_D at fixed values of either G or D are akin to those traditionally used in thermodynamics.

For the poor solvent a similar procedure gives the following values for $N > 200$,

$$\text{GSC: } A_G = 0.560 \pm 0.007, \quad \nu_G = 0.331 \pm 0.002 \quad \text{for } U^{(0)} = 7, \quad (19)$$

$$\text{GSC: } A_G = 0.516 \pm 0.004, \quad \nu_G = 0.333 \pm 0.001 \quad \text{for } U^{(0)} = 10, \quad (20)$$

$$\text{MC: } A_G = 0.60 \pm 0.004, \quad \nu_G = 0.31 \pm 0.02 \quad \text{for } U^{(0)} = 6, \quad (21)$$

or, roughly speaking, $\nu_G \approx \nu = \frac{1}{3}$, with coefficient A_G decreasing slowly with increasing $U^{(0)}$ and being almost independent of other parameters such as G . Hence, we have for a poor solvent,

$$\sqrt{3\mathcal{R}_g^2} \sim N^\nu \sim D^{\nu_G} (F-1)^{\nu_D (G+1)}, \quad \nu_D = \nu_G \simeq \nu = \frac{1}{3}. \quad (22)$$

It is interesting to note that for the ideal chain (absence of the excluded volume interactions, $d^{(0)} = 0$) we obtain the following accurate asymptotic expression³⁶ for large D and G ,

$$\sqrt{3\mathcal{R}_g^2} \simeq \ell \sqrt{3} D^{1/2} G^{1/2}. \quad (23)$$

Therefore, generally, the dependence of the radius of gyration on the spacer exponent is always the same as for an open/ring chain, but the ideal system lacks the complicated dependence on the number of generations G . It is worthwhile to comment also that such ideal system should not be confused with the system in the theta-solvent near the transition point $U_{\mathcal{E}'}^{(0)}$. For the latter we shall have a scaling akin to Eqs. (18,22),

$$\sqrt{3\mathcal{R}_g^2} \sim D^{\nu_G} (F-1)^{\nu_D (G+1)}, \quad \nu_G = \frac{1}{2}, \quad \nu_D \leq \nu_D \leq \nu_D. \quad (24)$$

The values for ν_G , ν_D obtained from the GSC theory are reported in Tabs. II,III. We can conclude that indeed $\nu_G = 1/2$ with a high accuracy, whereas $\nu_D \simeq 0.35$. We expect the latter to be somewhat lower in the MC simulation than in the GSC theory again.

V. DISCUSSION AND CONCLUSION

In this paper we have studied a range of homo- dendrimers with $D = 1 - 6$ spacers and $G = 1 - 7$ generations in the good and poor solvents, as well as across the coil-to-globule transition. These studies have been performed by two different techniques yielding a satisfactory agreement between their results. The first technique is based on the Gaussian self-consistent (GSC) method, while the second one is that of Monte Carlo (MC) simulation in continuous space. Both rely on the same coarse-grained model involving harmonic springs for connected monomers and the Lennard-Jones pair-wise potential with a hard core part. The overall accord between these two rather distinct approaches is quite important due to the limitations of both techniques. The MC technique, while in principle exactly modelling a given system, in practice is always limited by the statistical accuracy and quality of equilibration for very large dendrimers computationally affordable. The GSC method, on the other hand, is about 10^3 faster for the studied range of dendrimer sizes and it directly produces the ensemble averaged equilibrium observables. However, it is only an approximate technique, which has some intrinsic inaccuracies, for instance somewhat overestimating the size of polymers in the good solvent.

We have proposed a new scaling law for the radius of gyration of dendrimers which involves the two exponents ν_G (at fixed G) and ν_D (at fixed D),

$$\mathcal{R}_g \sim D^{\nu_G} (F - 1)^{\nu_D(G+1)} \sim D^{\nu_G - \nu_D} N^{\nu_D}, \quad (25)$$

where $\nu_G = \nu$, with $\nu \approx 3/5$, $1/2$, and $1/3$ being the inverse fractal dimension of an open/ring chain in the good, ideal and poor solvents respectively. While this agrees with the conclusions of Refs. 25,26 for ν_G , we have obtained a rather different dependence on the number of generations. Namely, we have concluded that $\nu_D \approx \nu - 1/4 \simeq 0.338$ for the good solvent, and $\nu_D \approx \nu = 1/3$ for the globule. This is consistent with Ref. 27, but our estimate of ν_D for the good solvent is more accurate enabling us to claim that ν_D is certainly above, although quite close to the poor solvent value $1/3$.

It is important to emphasise also that the law in Eq. (25) is valid for the model with the harmonic bonds employed here. Dendrimers with bonds possessing a finite stretchability and angular potentials would in all likelihood have more complicated and non-universal features in their behaviour. However, the harmonic model is an important and well tractable reference point for further studies at the level of full atomistic detail for concrete dendrimers, which could have bonds stretchable in different ranges.

We have concluded that the coil-to-globule transition for dendrimers is continuous and that for the theta-solvent the scaling law for \mathcal{R}_g differs from that of the ideal dendrimer, in which $\mathcal{R}_g \sim (DG)^{1/2}$, having instead the G -dependence of the form given by Eq. (25) with $1/3 \leq \nu_D \leq 3/5 - 1/4$.

Details of the conformational structure of dendrimers have been analysed for the good and poor solvents also. In some respects, our results support certain observations of Ref. 24 made for the good solvent. Namely, we find a strong evidence of the re-entry of the terminal generation into the dendrimer up to its very centre, producing a rather delocalised partial density for those monomers. This results in the highest total density near the core for relatively small dendrimers, which decreases in larger dendrimers due to the ‘entropic pull’ effect of extra branches. However, as the number of generations exceeds $G = 5$ there also develops a lower density domain inside the dendrimer. Moreover, we have analysed the bond stretching along a continuous branch. This is highest near the core, especially for dendrimers with a large number of generations. The stretching decreases with increasing generation index and oscillates in the magnitude with the spacer index. This observation is interpreted consistently with the connectivity contribution to the mean energy.

Furthermore, we have attempted to elucidate the degree of the steric congestion in a dendrimer by considering the shell index dependence of the monomer packing coefficient η_ρ . The latter is the volume ratio of the space occupied by all other monomers around a given one. In a relatively small dendrimer η_ρ oscillates in the spacer index with only a weak generation index dependence, except for the terminal generation which is less congested. A dendrimer with a large number of generations, however, has a less congested hollow domain inside it and the highest congestion in the penultimate generations in accord with the density distributions.

The degree of asphericity of dendrimers appears to decrease with the increasing number of generations, depending rather weakly on the number of spacers. This is also confirmed by the behaviour of the static structure factor, which develops an oscillating globule-like character for larger G .

Interestingly, while incorrect in concrete detail, the onion model predictions of Ref. 13 do have a rather limited meaning in a sense that there exists a hollow domain inside a dendrimer of large enough number of generations, but not at the core itself. However, the partial densities of generations fall off only beyond the appropriate cut-off radii. These densities are totally delocalised until the cut-offs (see Fig 6b), being fairly large at the core²⁷, and certainly are not concentrated within thin layers as surmised.

A similar analysis has been carried out for the poor solvent as well. The globular conformation of a dendrimer is much more compact, and it is rather uniform without any hollow domains. The packing coefficient for the globule is much larger in value than for the good solvent and depends on the spacer index only for the monomers in the inner generations. There is also much less stretching of bonds involved near the core than for the good solvent, even in a dendrimer with a large G . Generally, the bond stretching in the globule is stronger for the branch points than for the middle of spacers or terminal monomers. Thus, the connectivity of a dendrimer in the globular state manifests itself in a much more localised manner, and with a significantly smaller effect than for the good solvent.

We believe that our results allow one to reconcile some of the disparate predictions from previous theoretical and simulation studies by finding some simple limiting regimes and by discovering non-monotonic dependencies of various observables and the local structure of dendrimers on the number of generations. These unusual features of dendrimers indeed make them extremely appealing for numerous future applications ranging from catalysis, rheology modifiers, to drug delivery and biotechnology more generally.

ACKNOWLEDGMENTS

The authors acknowledge interesting discussions with Professor G. Allegra, Dr G. Raos, and particularly with Professor F. Ganazzoli who attracted our attention to the field of dendrimers. We are also grateful to Gillian Flanagan and Marese O'Brien for their help and insight during their undergraduate research projects. Support from the IRCSET basic research grant SC/02/226 is also acknowledged.

APPENDIX A: THE TOPOLOGICAL TREE

The concept of the kinematic symmetries can be best explained by using the topological tree presented in Fig. 16, which is equivalent to the dendrimer diagram of Fig. 1. Hence, the horizontal line would represent any selected consecutive branch of the dendrimer, which we shall name the primary branch \mathcal{B} , with the core monomer being on the left. The length of \mathcal{B} is then $n_{\mathcal{B}} = D(G + 1)$, excluding the core monomer itself. Any two branches become topologically non-equivalent to each other as long as they diverge from the common parent sub-branch at some value of the generation index g . We shall call any two such branches non-equivalent of order g . The leftmost vertical line on the left of Fig. 16 represents any branch non-equivalent to \mathcal{B} of order $g = 0$, which we shall denote as \mathcal{B}_0 with the length $n_{\mathcal{B}_0} \equiv n_0$. Similarly then, we shall have branches \mathcal{B}_g non-equivalent to \mathcal{B} of order g with the length $n_g = D(G - g + 1)$ for all values of $g = 0, 1, \dots, G$ in our topological tree. Any two pairs of monomers then would have $\mathcal{D}_{ij} = \mathcal{D}_{i'j'}$ as long as the pair (i', j') lies in the same places in the topological tree as the pair (i, j) , thereby defining the equivalence classes of monomer pairs.

Moreover, we can easily count the number of independent degrees of freedom in the matrix \mathcal{D}_{ij} . For that we have to count the number of possible pairs (ρ, ρ') in Fig. 16 such that e.g. $\rho' \leq \rho$, where $i = (\rho, \varphi)$ and $i' = (\rho', \varphi')$. Accidentally, we note that the topological tree disregards the angular coordinates φ of any equivalent monomers. There are two possibilities of pairing ρ and ρ' : a) $\rho, \rho' \in \mathcal{B}$ and b) $\rho \in \mathcal{B}$ and $\rho' \in \mathcal{B}_g$ for some g . In the former case we get the number of pairs $C_{\mathcal{B}} = \sum_{i=1}^{n_{\mathcal{B}}} i = n_{\mathcal{B}}(n_{\mathcal{B}} + 1)/2$, whereas in the latter case we obtain $C_g = \sum_{i=n_g}^1 i = n_g(n_g + 1)/2$. Thus, we have derived the total number of independent degrees of freedom,

$$C_{ind}^{(2)} = C_{\mathcal{B}} + \sum_{g=G}^0 C_g = (G + 1) \frac{D}{2} \left(D \left(\frac{G^2}{3} + \frac{13}{6}G + 2 \right) + 2 + \frac{G}{2} \right), \quad (\text{A1})$$

which is identical to Eq. (A-1) in Ref. 19.

Similarly, the total number of independent 1-point observables (e.g. the packing coefficient η_i), which depend on ρ only, is simply the length of the primary branch \mathcal{B}_0 ,

$$C_{ind}^{(1)} = D(G + 1) + 1. \quad (\text{A2})$$

¹ A. Hult, M. Johansson, E. Malmström. *Adv. Polym. Sci.* **143** 1 (1999).

- ² G.R. Newkome, C.N. Moorefield, F. Vögtle. *Dendritic Molecules*. Verlag-Chemie, Weinheim, Germany (1996).
- ³ D.A. Tomalia, A.N. Naylor, W.A. Goddard III. *Angew. Chem. Int. Ed. Engl.* **29** 138 (1990).
- ⁴ J.M.J. Fréchet. *Science* **263** 1710 (1994).
- ⁵ A.W. Bosman, H.M. Janssen, E.W. Meijer. *Chem. Rev.* **99** 1665 (1999).
- ⁶ G.E. Oosterom, J.N.H. Reek, P.C.J. Kamer, P.W.N.M. van Leuwen. *Angew. Chem. Int. Ed.* **40** 1829 (2001).
- ⁷ D. de Groot, B.F.M. de Waals, J.N.H. Reek, A.P.H.J. Schenning, P.C.J. Kamer, E.W. Meijer, P.W.N.M. van Leuwen. *J. Am. Chem. Soc.* **123** 8453 (2001).
- ⁸ M. Liu, J.M.J. Fréchet. *Pharm. Sci. Technol. Today* **2** (10) 393 (1999).
- ⁹ J.F.G.A. Jansen, E.M.M. de Brabander-van den Berg, E.W. Meijer. *Science* **266** 1226 (1994).
- ¹⁰ R. La Ferla. *J. Chem. Phys.* **106** 688 (1997).
- ¹¹ J.J. Freire. *Adv. Polym. Sci.* **143** 34 (1999).
- ¹² R. Scherrenberg, B. Coussens, P. van Vliet, G. Edouard, *et al.* *Macromol.* **31** 456 (1998); F. Mallamace, E. Canetta, D. Lombardo, A. Mazzaglia, *et al.* *Physica A* **304** 235 (2002).
- ¹³ P.G. de Gennes, H. Hervet. *J. Phys. (Paris)* **44** L351 (1983).
- ¹⁴ D. Boris, M. Rubinstein. *Macromol.* **29** 7251 (1996).
- ¹⁵ F. Ganazzoli. *Cond. Matter Phys.* **5** 1 (2002).
- ¹⁶ E.G. Timoshenko, Yu.A. Kuznetsov, K.A. Dawson. *Phys. Rev.* **E 57** 6801 (1998).
- ¹⁷ M. Doi, S.F. Edwards. *The Theory of Polymer Dynamics*. Oxford Science, New York (1989).
- ¹⁸ J. des Cloiseaux, G. Jannink. *Polymers in Solution*. Oxford Science Publ. (1990).
- ¹⁹ F. Ganazzoli, R. La Ferla, G. Terragni. *Macromol.* **33** 6611 (2000).
- ²⁰ F. Ganazzoli, R. La Ferla, G. Raffaini. *Macromol.* **34** 4222 (2001).
- ²¹ F. Ganazzoli, R. La Ferla. *J. Chem. Phys.* **113** 9288 (2000).
- ²² A.N. Naylor, W.A. Goddard III, G.E. Kiefer, D.A. Tomalia. *J. Am. Chem. Soc.* **111** 2339 (1989).
- ²³ R.L. Lescanec, M. Muthukumar. *Macromol.* **23** 2280 (1990).
- ²⁴ M.L. Mansfield, L.I. Klushin. *Macromol.* **26** 4262 (1993).
- ²⁵ Zh.Yu. Chen, Sh.-M. Cui. *Macromol.* **29** 7943 (1996).
- ²⁶ P. Biswas, B.J. Cherayil. *J. Chem. Phys.* **100** 3201 (1994).
- ²⁷ M. Murat, G.S. Grest. *Macromol.* **29** 1278 (1996).
- ²⁸ Yu.A. Kuznetsov, E.G. Timoshenko. *J. Chem. Phys.* **111**, 3744 (1999).
- ²⁹ F. Ganazzoli, Yu.A. Kuznetsov, E.G. Timoshenko. *Macromol. Theory Simul.* **10** 325 (2001).
- ³⁰ E.G. Timoshenko, Yu.A. Kuznetsov, R. Connolly. *J. Chem. Phys.* **116** 3905 (2002).
- ³¹ We have used the 28-CPU Beowulf cluster (SCOP) described in detail at <http://darkstar.ucd.ie/cluster>.
- ³² E.G. Timoshenko, Yu.A. Kuznetsov. Accepted for publication in *J. Chem. Phys.* **117**: 11 issue 15th of Sep. AIP ID 503235JCP (2002); E-print: cond-mat/0207204.
- ³³ E.G. Timoshenko, Yu.A. Kuznetsov. *Colloids and Surfaces A* **190** 135 (2001).
- ³⁴ M.P. Allen and D.J. Tildesley (Ed.), *Computer Simulation of Liquids*. Clarendon Press, Oxford (1987).
- ³⁵ N.F. Carnahan, K.E. Starling. *J. Chem. Phys.* **51** 635 (1969).
- ³⁶ For $d^{(0)} = 0$ the GSC theory and MC simulations exactly agree with the analytic formula for \mathcal{R}_g^2 by La Ferla¹⁰. Note that we do not have a factor of 3 in the first term of Eq. (1) and that the mean-squared radius of gyration in our notation is the quantity $3\mathcal{R}_g^2$. Both of the factors of 3 cancel out therefore, so that formally $\mathcal{R}_g^2(\text{our}) = \mathcal{R}_g^2(\text{La Ferla})$.

APPENDIX: FIGURE CAPTIONS

FIG. 1. Schematic connectivity diagram of the dendrimer D2G3. Here dashed circles denote different generations, big filled circles correspond to the branch points and the triangle is the core monomer. Notations for the indices d, ρ, φ and for some selected monomers, which are numbered in the clock-wise and outwards manner, are also introduced.

FIG. 2. Plots of the mean-squared radius of gyration $3\mathcal{R}_g^2$ vs the number of generations G for the dendrimers in the good solvent ($U^{(0)} = 0$) from the GSC theory (filled circles and thin lines) and from the MC simulation (empty circles and thick lines). The curves (from bottom to top) correspond to the following values: $D = 1$ (GSC), 2 (MC), 2 (GSC), 4 (MC), 4 (GSC), 6 (GSC). The largest relative statistical error, $\delta R_g^2 = \Delta R_g^2 / R_g^2 \cdot 100\%$, in this plot occurs for the D2G7 dendrimer and equals 0.1%.

FIG. 3. Plots of the mean ratios of the eigenvalues of the shape tensor $\lambda^{(a)}$ vs the number of generations G for the dendrimers in the good solvent ($U^{(0)} = 0$) from MC simulation. Solid curves correspond to $D = 2$ and empty circles to $D = 4$. The largest relative statistical errors, $\delta \lambda^{(a)} = \Delta \lambda^{(a)} / \lambda^{(a)} \cdot 100\%$, in this plot occur for the D2G7 dendrimer and are equal to: $\delta \lambda^{(1)} = 0.15\%$, $\delta \lambda^{(2)} = 0.2\%$ and $\delta \lambda^{(3)} = 0.3\%$.

FIG. 4. Typical snapshots of conformations of the dendrimers D3G3 (Fig. a) and D3G7 (Fig. b) in the good solvent from MC simulation. The core monomer is represented as a sphere of the monomer real diameter $d^{(0)} = \ell$ in both figures.

FIG. 5. Kratky plots of the rescaled static structure factor $\hat{S} = p^2 3\mathcal{R}_g^2 S(p) / N$ vs the rescaled wave number $\hat{p} = p \sqrt{3\mathcal{R}_g^2}$ for dendrimers in the good solvent ($U^{(0)} = 0$) from MC simulation. Here the solid line corresponds to D1G5, the long-dashed curve — to D1G6 and the short-dashed curve — to D2G5 dendrimer. The largest relative statistical errors in this plot occur for the D2G5 dendrimer and are equal to: $\delta \hat{p} = 0.1\%$ and $\delta \hat{S} \leq 0.3\%$.

FIG. 6. Plots of the monomer densities $g_g^{(1)}$ vs the separation from the centre-of-mass \mathbf{r}_{cm} for the dendrimers D2G4 (Fig. a) and D2G6 (Fig. b) in the good solvent ($U^{(0)} = 0$) from MC simulation. Insets of figures show the monomer densities of the same dendrimers in the poor solvent ($U^{(0)} = 6$). Curves from top to bottom as on the left-hand side correspond to the following densities. In main bodies of figures: the total density $\sum_g g_g^{(1)}$ (solid line), density of non-terminal generations $\sum_{g < G} g_g^{(1)}$ (dashed line), density of the innermost generations $g_{-1}^{(1)} + g_0^{(1)}$ (thin solid line with quadrangles), density of the terminal generation $g_G^{(1)}$ (dotted line), and density of the penultimate generation $g_{G-1}^{(1)}$ (thin line with triangles); In insets of figures: the total density $\sum_g g_g^{(1)}$ (solid line), density of non-terminal generations $\sum_{g < G} g_g^{(1)}$ (dashed line), density of the terminal generation $g_G^{(1)}$ (dotted line). Errorbars represent statistical errors of the data from MC simulation.

FIG. 7. Plots of the mean-squared distances $D_{(\rho-1,0)(\rho,0)}$ between radial nearest neighbours vs the shell index ρ from MC simulation (main body of the figure) and from the GSC theory (inset of the figure) for dendrimers with $D = 2$ spacers in the good solvent ($U^{(0)} = 0$). The curves correspond to $G = 1, 2, 3, 4, 5, 6, 7$ (from bottom to top). Errorbars represent statistical errors of the data from MC simulation.

FIG. 8. Plots of the mean-squared distances $D_{(\rho-1,0)(\rho,0)}$ vs the shell index ρ from MC simulation (main body of the figure) and from the GSC theory (inset of the figure) for dendrimers with $D = 4$ spacers in the good solvent ($U^{(0)} = 0$). The curves correspond to $G = 1, 2, 3, 4, 5, 6$ (from bottom to top). Errorbars represent statistical errors of the data from MC simulation.

FIG. 9. Plots of the mean-squared distances $D_{(\rho-1,0)(\rho,0)}$ vs the shell index ρ from the GSC theory for dendrimers with $D = 6$ spacers in the good solvent ($U^{(0)} = 0$). The curves correspond to $G = 1, 2, 3, 4, 5, 6$ (from bottom to top).

FIG. 10. Plots of the packing coefficient η_ρ defined by Eqs. (8,9) vs the rescaled shell index ρ/D for dendrimers consisting of $G = 6$ generations in the good solvent ($U^{(0)} = 0$) from the GSC theory. The curves correspond to the following values of $D = 1, 2, 3, 4, 6$ (from top to bottom).

FIG. 11. Plots of the packing coefficient η_ρ vs the shell index ρ for dendrimers with $D = 3$ spacers in the good solvent ($U^{(0)} = 0$) from the GSC theory. The curves correspond to the following values of G : $G = 1$ (dotted line), $G = 3$ (short-dashed line), $G = 5$ (long-dashed line), and $G = 7$ (solid line).

FIG. 12. Plots of the mean-squared radius of gyration $3\mathcal{R}_g^2$ (Fig. a) and the specific energy slope $N^{-1}d\mathcal{E}/dU^{(0)}$ (Fig. b) vs the degree of Lennard-Jones attraction $U^{(0)}$ across the coil-to-globule transition from the GSC theory for dendrimers with $G = 5$ generations and $D = 1, 2, 3, 4, 6$ (from bottom to top as on the left-hand side).

FIG. 13. Plots of the mean-squared radius of gyration $3\mathcal{R}_g^2$ vs the number of generations G for the dendrimers in the poor solvent, $U^{(0)} = 7$, from the GSC theory (filled circles and solid lines) and for the ideal dendrimers, $d^{(0)} = 0$ (filled quadrangles and dashed lines). The curves correspond to the following values of D for each of the two families: $D = 1, 2, 3, 4, 5, 6$ (from bottom to top).

FIG. 14. Plots of the mean-squared distances $D_{(\rho-1,0)}(\rho,0)$ vs the shell index ρ from the GSC theory for dendrimers with $D = 6$ spacers in the poor solvent ($U^{(0)} = 7$). The curves correspond to $G = 1, 2, 3, 4, 5, 6$ (from bottom to top).

FIG. 15. Plots of the packing coefficient η_ρ vs the shell index ρ for dendrimers with $D = 6$ spacers in the poor solvent ($U^{(0)} = 7$) from the GSC theory. The curves correspond to the following values of $G = 1, 2, 3, 4, 5, 6$ (from bottom to top).

FIG. 16. Tree diagram topologically equivalent to that of Fig. 1 for D2G3 dendrimer. Dotted line illustrates the area satisfying condition $\rho' \leq \rho$.

APPENDIX: TABLES

TABLE I. Values of the pair-wise interaction parameter at the coil-to-globule transition point $U_{\mathcal{E}'}^{(0)}$ and at the special point $U_{\mathcal{R}}^{(0)}$ in parentheses vs D and G . The former has been determined by a quadratic interpolation of the maxima positions of $-d^2\mathcal{E}/dU^{(0)2}$. The latter has been determined by the condition, $\mathcal{R}_g^2(U_{\mathcal{R}}^{(0)}) = \mathcal{R}_g^2(\text{ideal})$.

	$G = 1$	$G = 2$	$G = 3$	$G = 4$	$G = 5$	$G = 6$
$D = 1$	4.86 (4.28)	3.87 (3.81)	3.27 (3.75)	2.97 (4.02)	2.75 (4.78)	2.54 (6.97)
$D = 2$	4.05 (3.50)	3.24 (3.20)	2.87 (3.17)	2.70 (3.33)	2.61 (3.77)	2.50 (4.90)
$D = 3$	3.56 (3.17)	2.96 (2.95)	2.68 (2.92)	2.55 (3.03)	2.48 (3.36)	2.43 (4.14)
$D = 4$	3.29 (2.99)	2.80 (2.79)	2.57 (2.77)	2.45 (2.87)	2.39 (3.13)	2.36 (3.74)
$D = 5$	3.11 (2.86)	2.69 (2.70)	2.49 (2.67)	2.39 (2.75)	2.35 (2.98)	—
$D = 6$	2.98 (2.77)	2.61 (2.62)	2.43 (2.60)	2.35 (2.68)	2.31 (2.87)	—

TABLE II. Values of parameters a_G , ν_G and \mathbf{a}_G , \mathbf{v}_G obtained from fitting procedure via Eqs. (11,12) for the good athermal, $U^{(0)} = 0$, and the theta, $U_{\mathcal{E}'}^{(0)}$, solvents over various values of D at a given value of G from the GSC and MC methods.

G	GSC: a_G	ν_G	MC: a_G	ν_G	GSC: \mathbf{a}_G	\mathbf{v}_G
1	0.532 ± 0.009	0.615 ± 0.005	0.63 ± 0.01	0.55 ± 0.01	0.60 ± 0.02	0.477 ± 0.009
2	0.445 ± 0.007	0.626 ± 0.004	0.50 ± 0.03	0.58 ± 0.02	0.51 ± 0.02	0.489 ± 0.006
3	0.371 ± 0.005	0.629 ± 0.003	0.44 ± 0.03	0.57 ± 0.01	0.44 ± 0.02	0.500 ± 0.005
4	0.312 ± 0.004	0.628 ± 0.002	0.35 ± 0.01	0.58 ± 0.01	0.39 ± 0.01	0.498 ± 0.004
5	0.266 ± 0.004	0.624 ± 0.002	0.29 ± 0.02	0.59 ± 0.01	0.34 ± 0.01	0.501 ± 0.006
6	0.232 ± 0.003	0.621 ± 0.002	0.26 ± 0.01	0.57 ± 0.01	0.30 ± 0.01	0.497 ± 0.005

TABLE III. Values of parameters a_D , ν_D and \mathbf{a}_D , \mathbf{v}_D obtained from fitting procedure via Eqs. (11,12) for the good athermal, $U^{(0)} = 0$, and the theta, $U_{\mathcal{E}'}^{(0)}$, solvents over various values of G at a given value of D from the GSC and MC methods.

D	GSC: a_D	ν_D	MC: a_D	ν_D	GSC: \mathbf{a}_D	\mathbf{v}_D
1	0.98 ± 0.01	0.377 ± 0.002	1.08 ± 0.01	0.333 ± 0.002	0.69 ± 0.03	0.380 ± 0.006
2	1.18 ± 0.02	0.373 ± 0.002	1.29 ± 0.02	0.329 ± 0.002	0.85 ± 0.03	0.355 ± 0.005
3	1.33 ± 0.03	0.370 ± 0.003	1.43 ± 0.03	0.330 ± 0.003	0.92 ± 0.01	0.346 ± 0.003
4	1.42 ± 0.05	0.370 ± 0.004	1.50 ± 0.05	0.332 ± 0.004	0.96 ± 0.02	0.346 ± 0.003
5	1.52 ± 0.06	0.369 ± 0.005	1.48 ± 0.09	0.340 ± 0.007	0.97 ± 0.04	0.349 ± 0.006
6	1.60 ± 0.07	0.368 ± 0.005	1.62 ± 0.09	0.335 ± 0.008	1.00 ± 0.04	0.351 ± 0.005

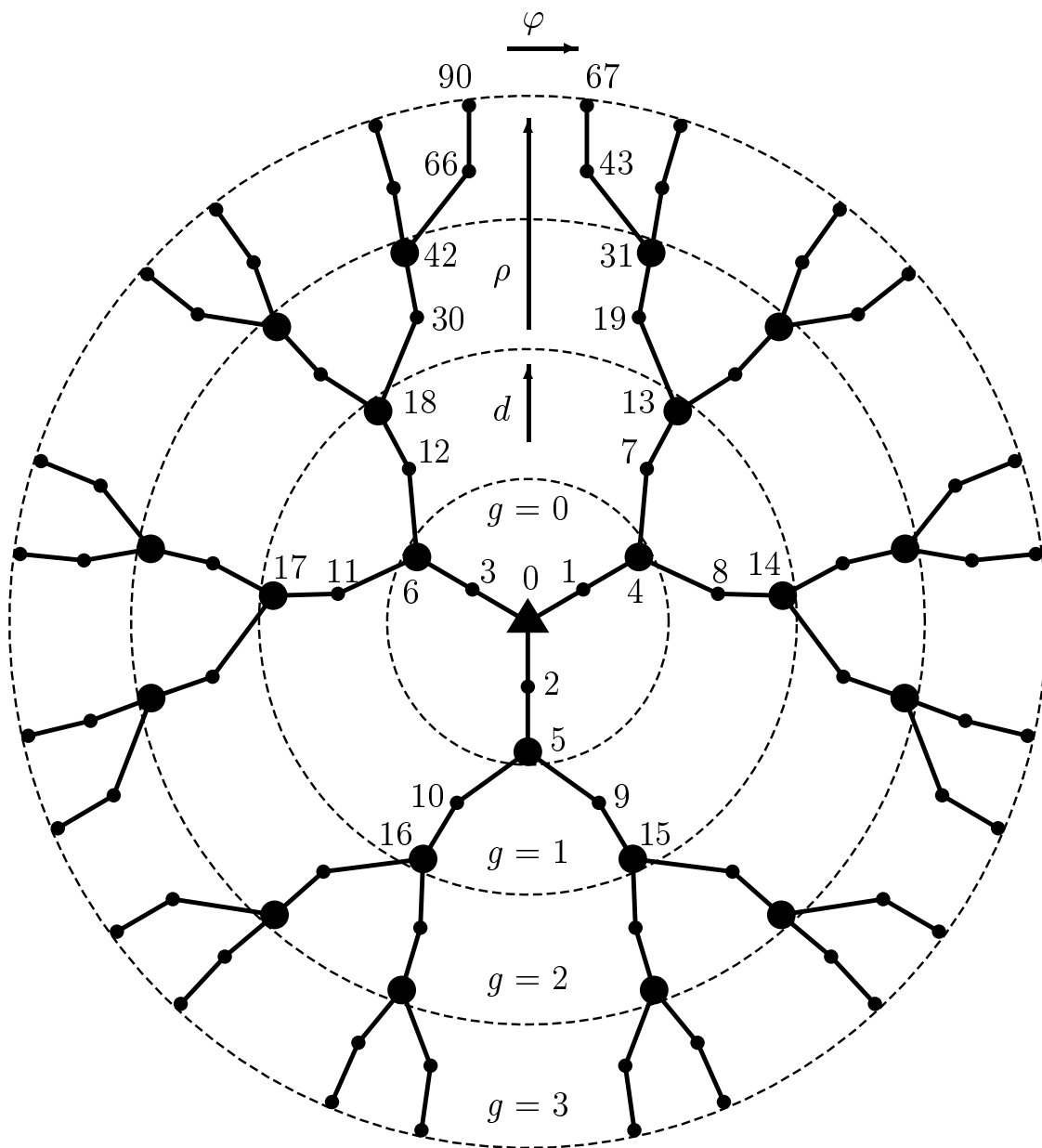


Fig. 1

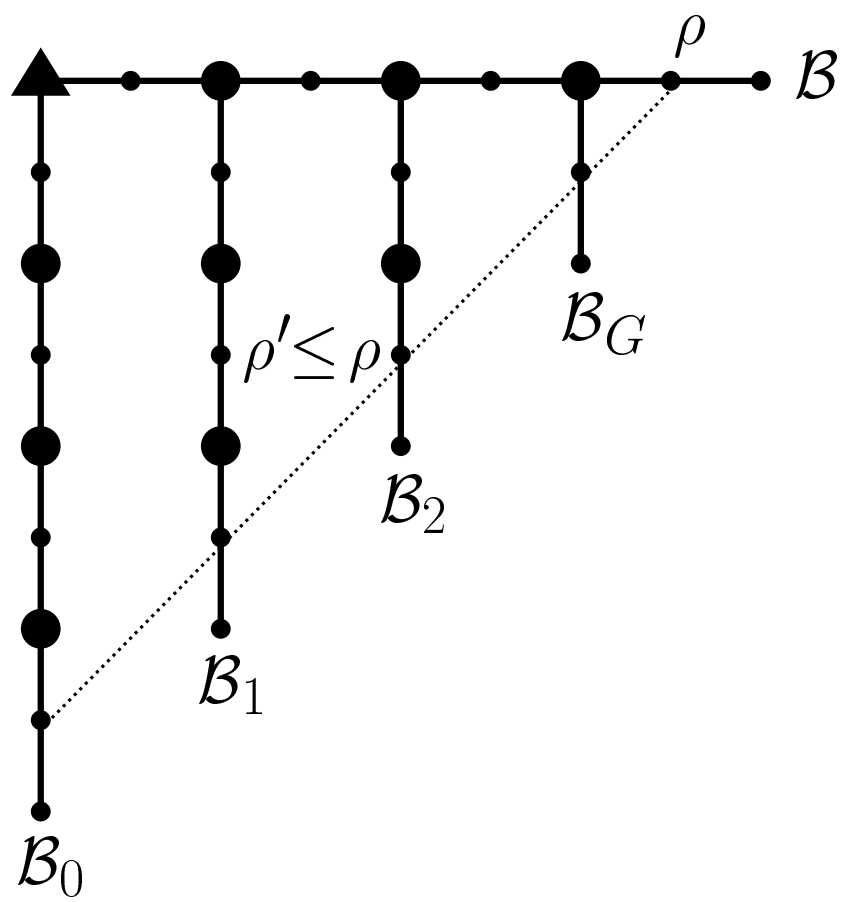


Fig. 16

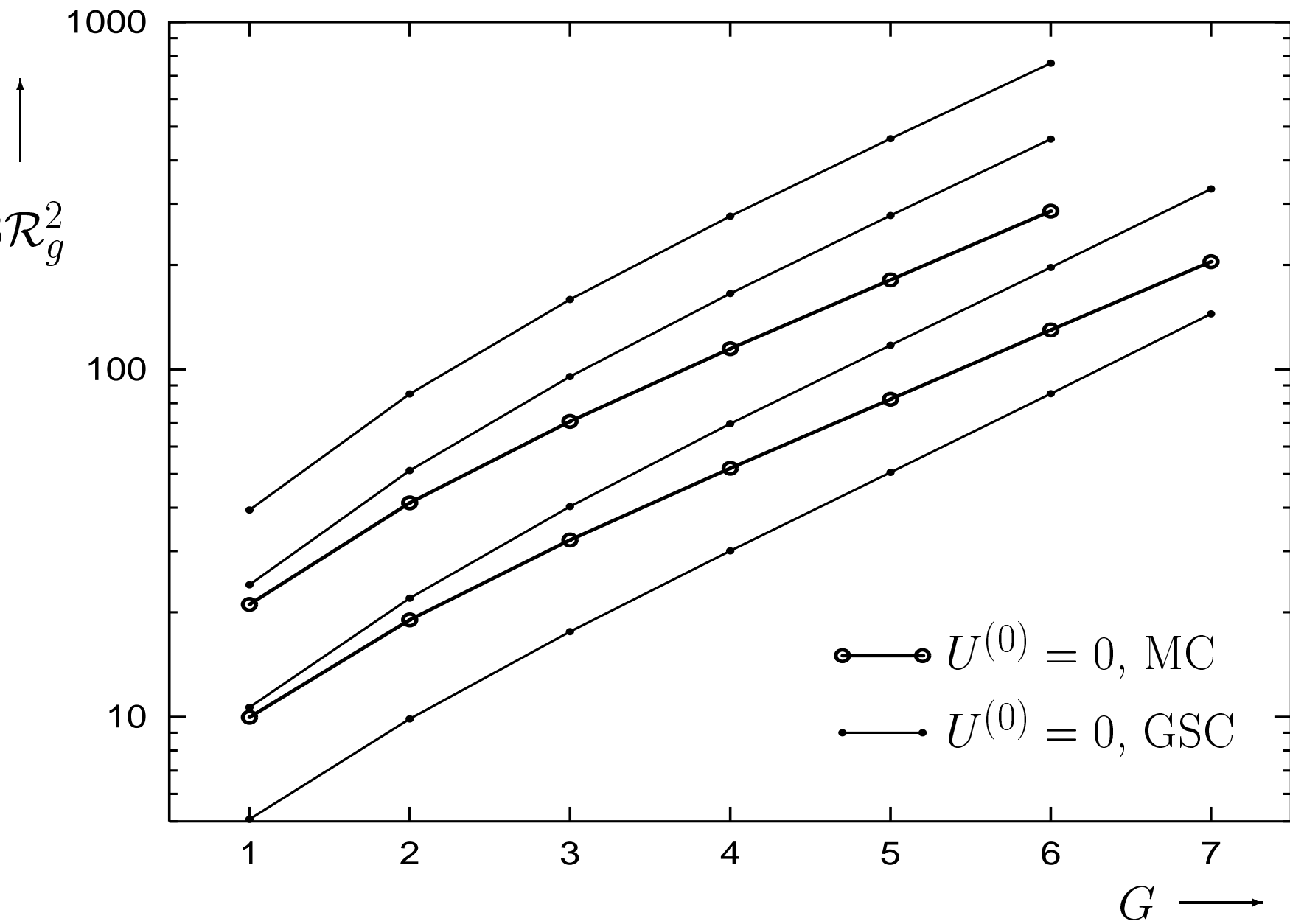


Fig. 2

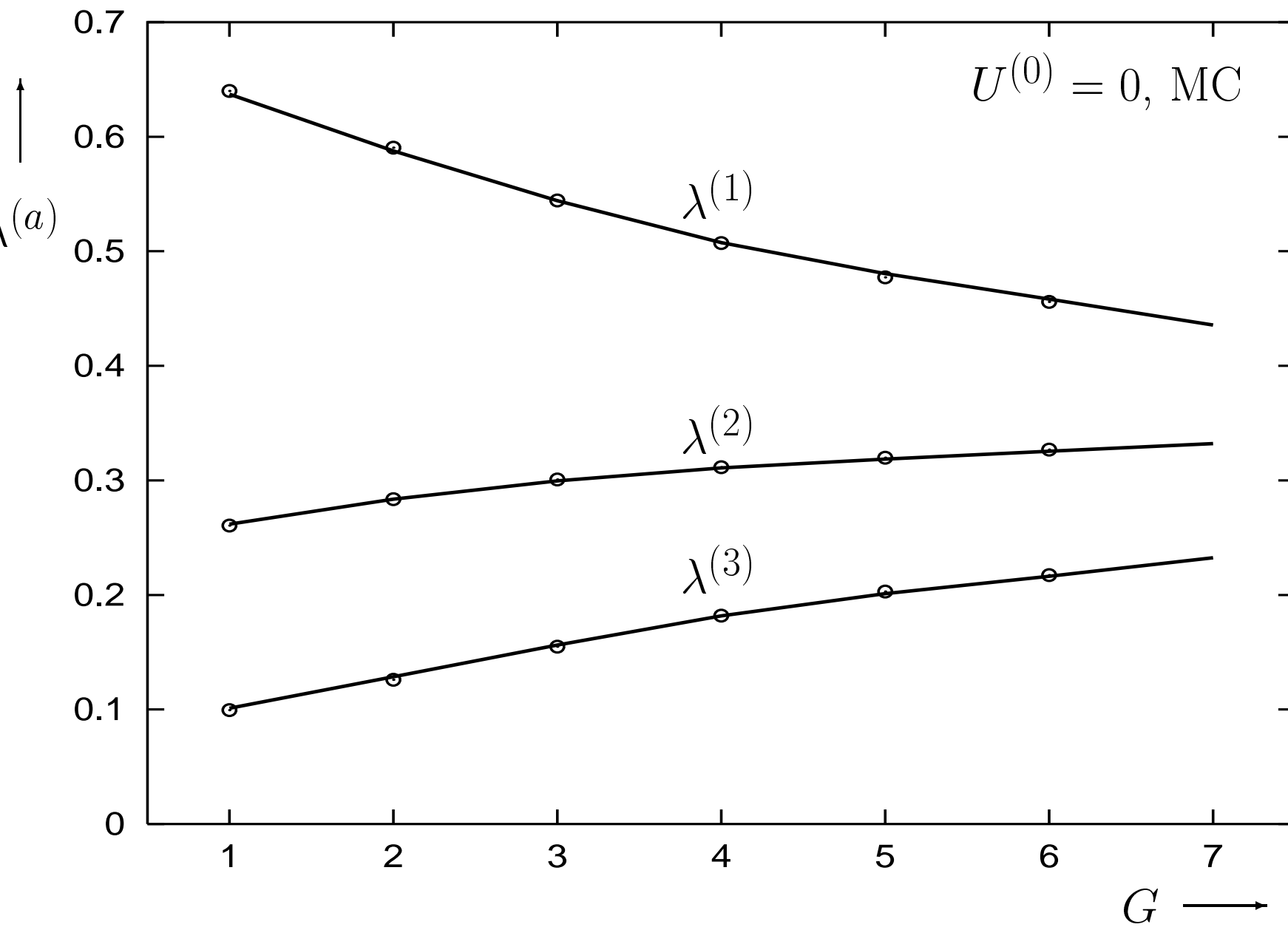


Fig. 3

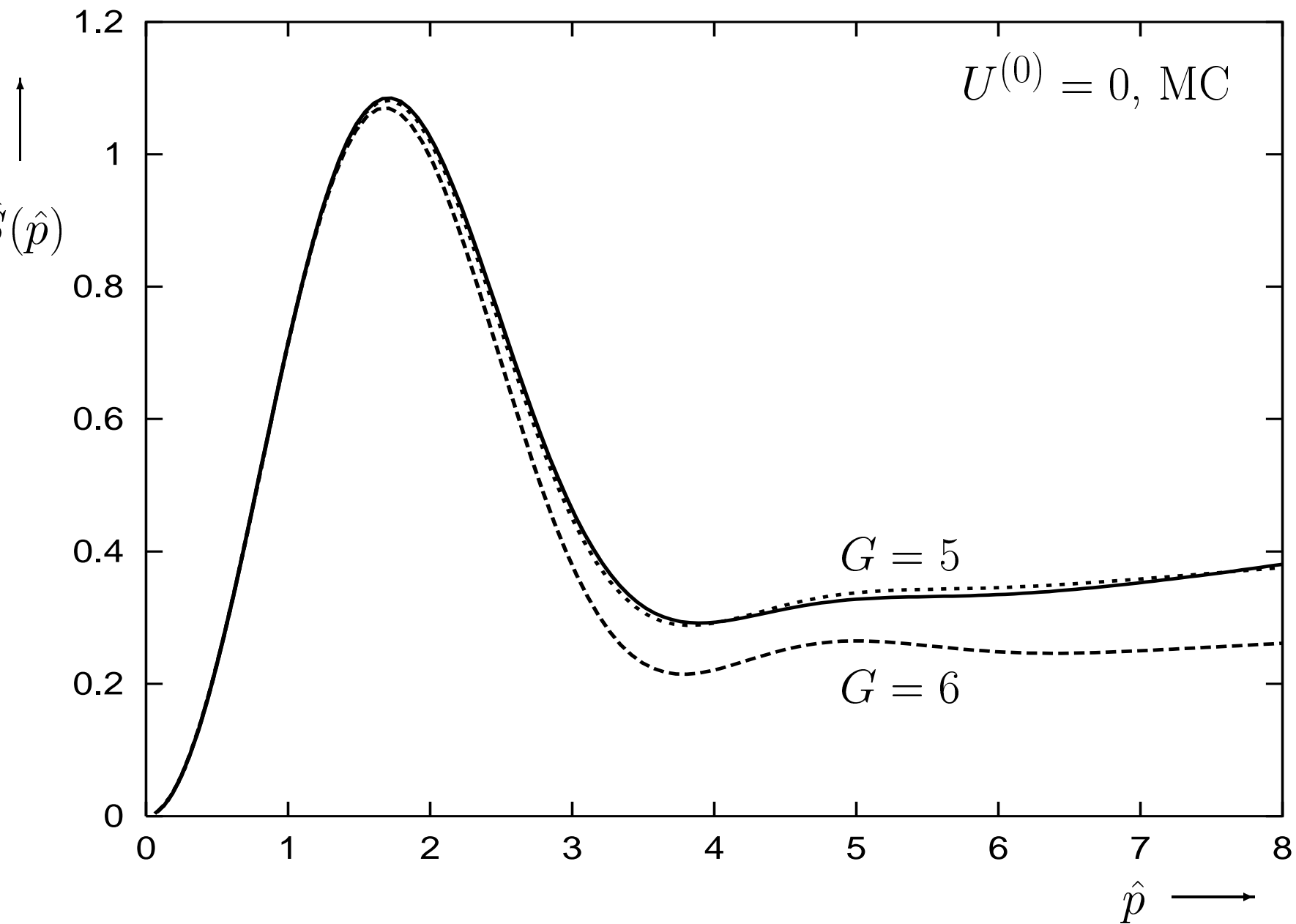


Fig. 5

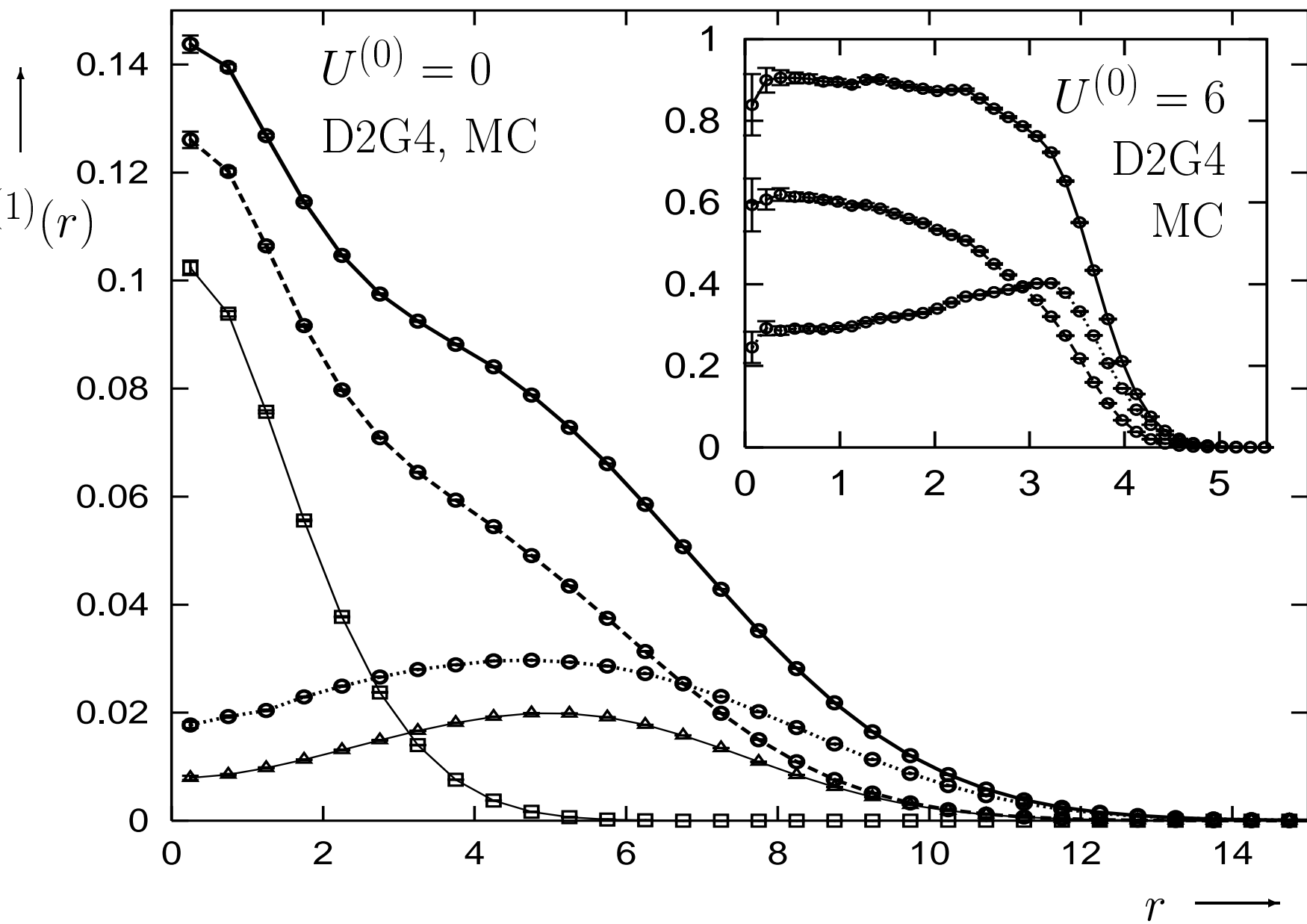


Fig. 6a

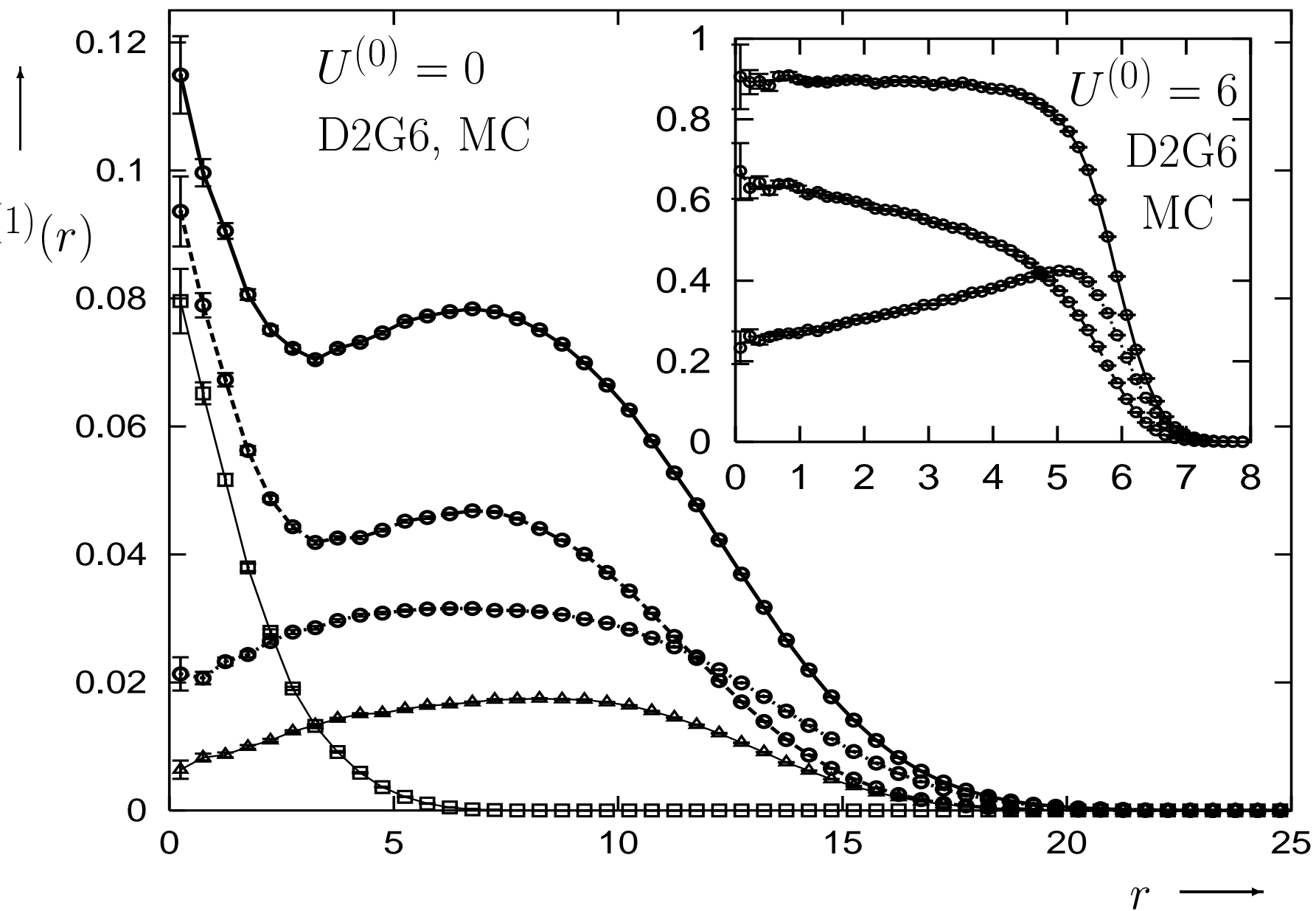


Fig. 6b

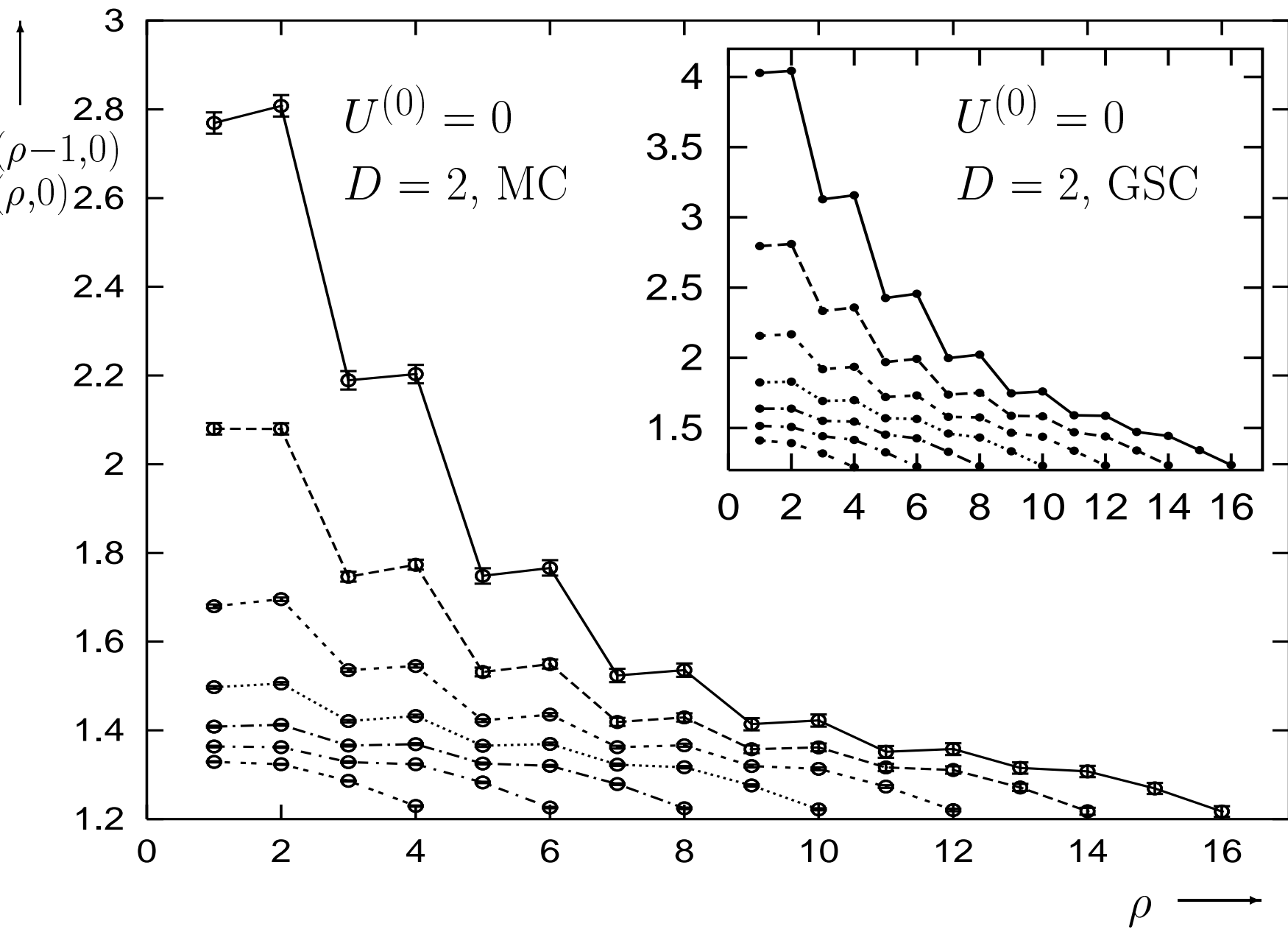


Fig. 7

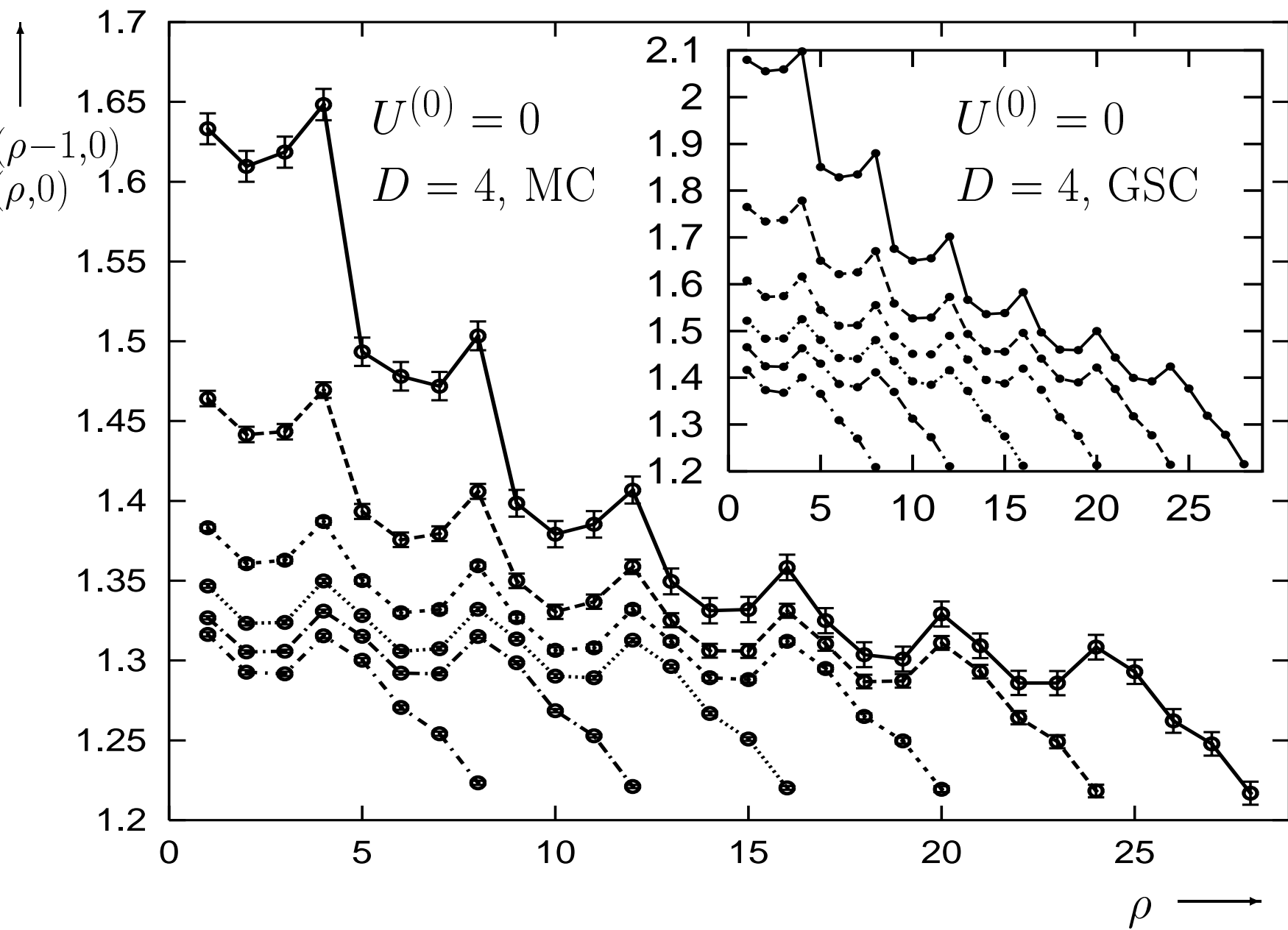


Fig. 8

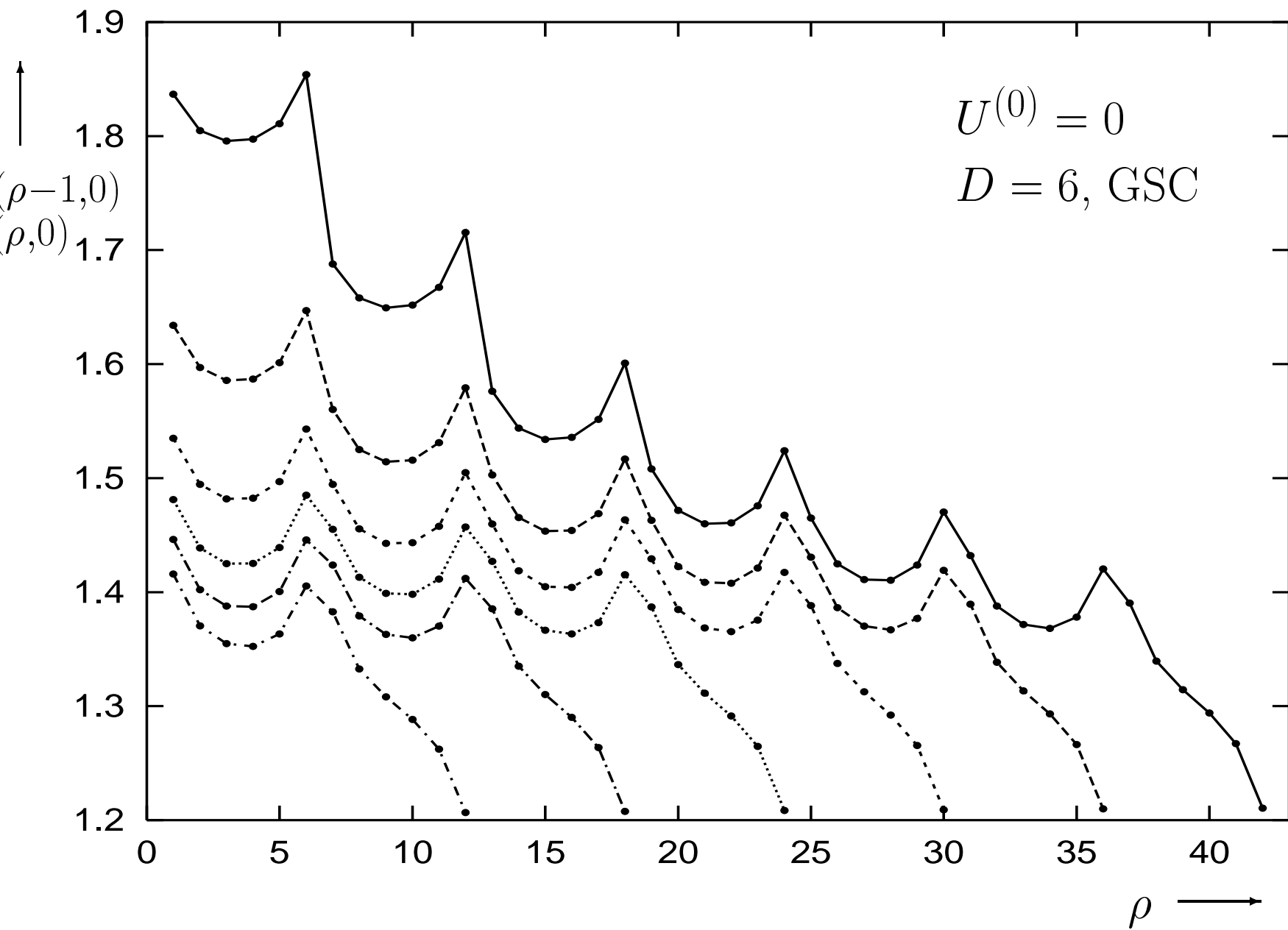


Fig. 9

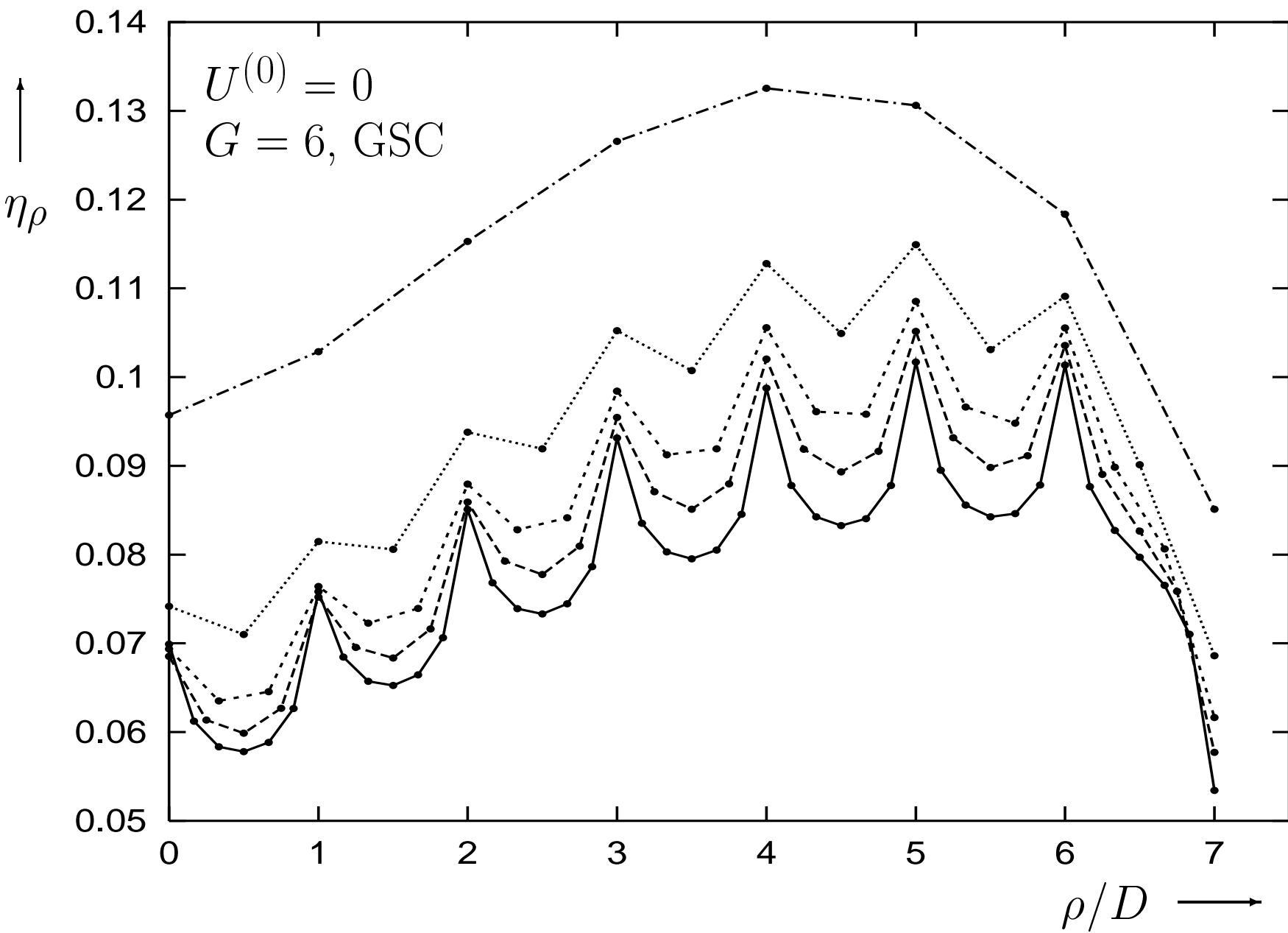


Fig. 10

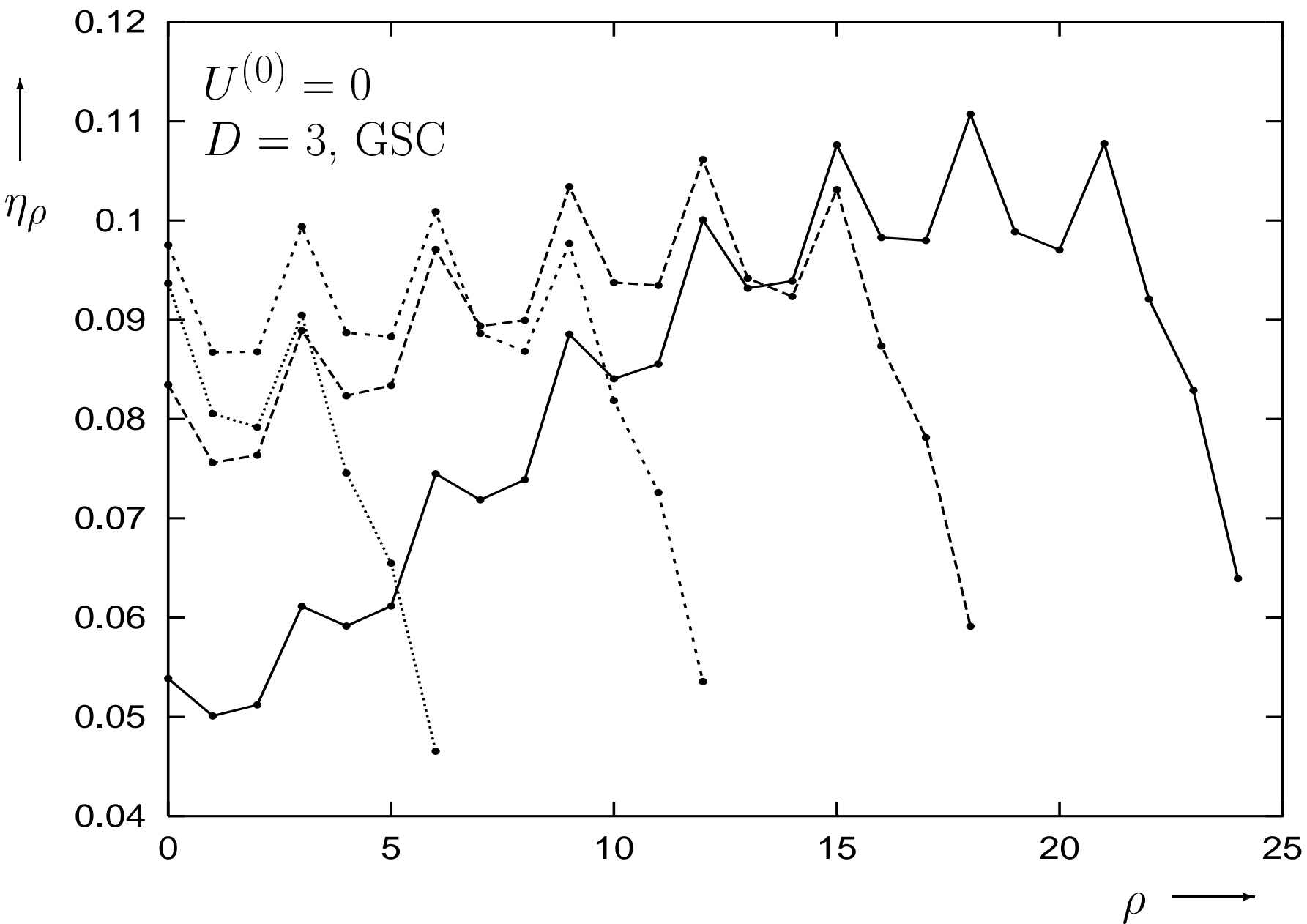


Fig. 11

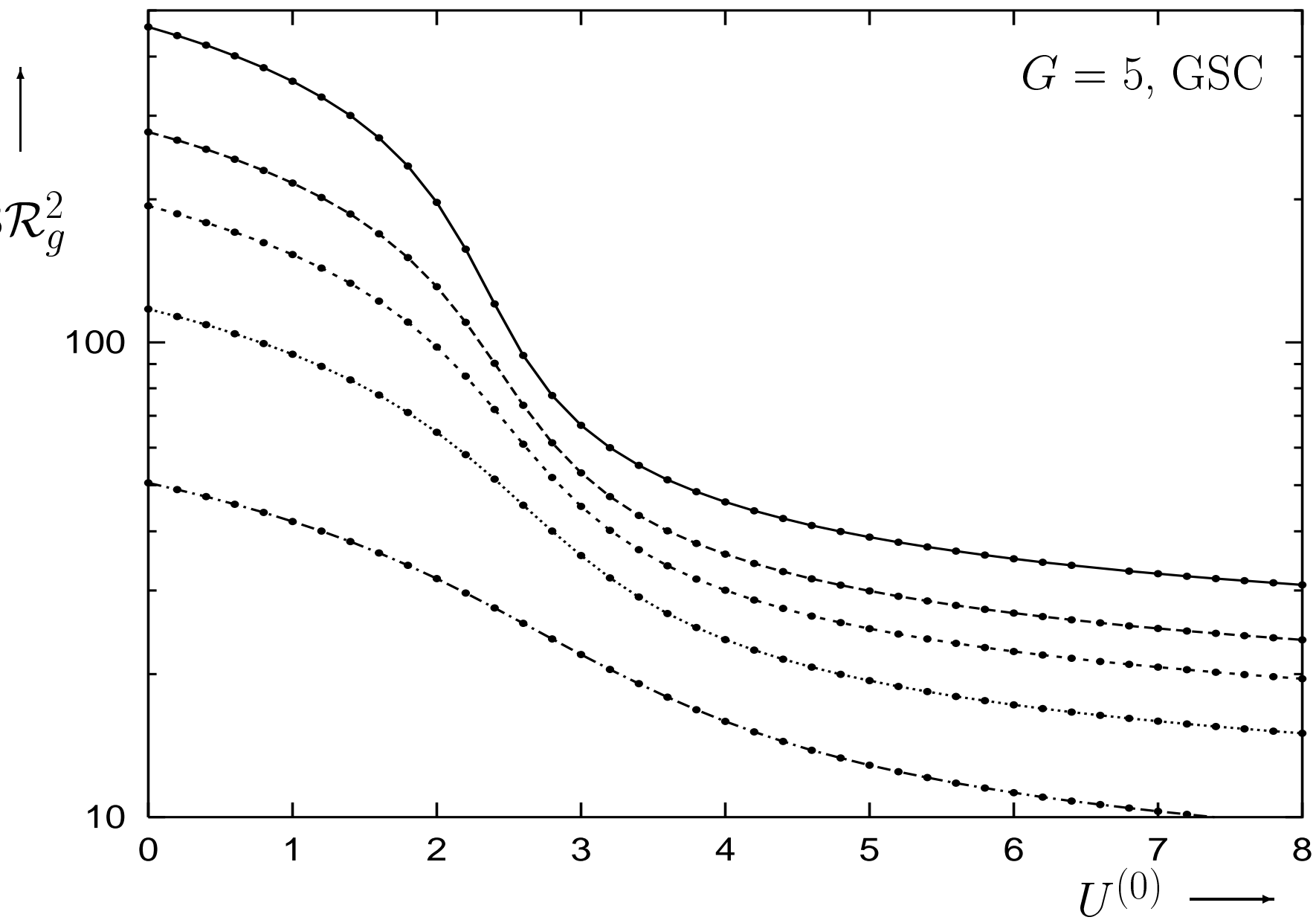


Fig. 12a

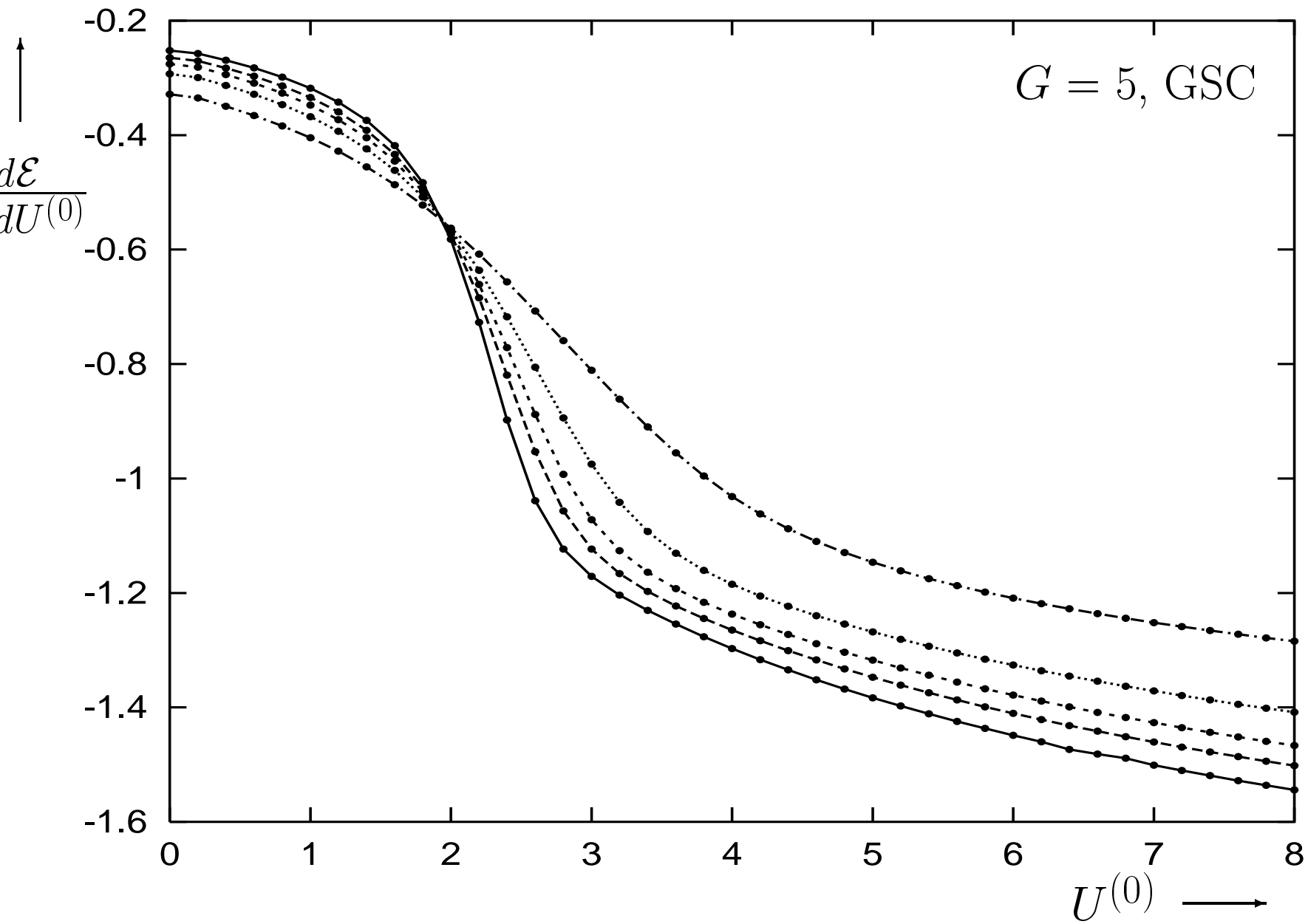


Fig. 12b

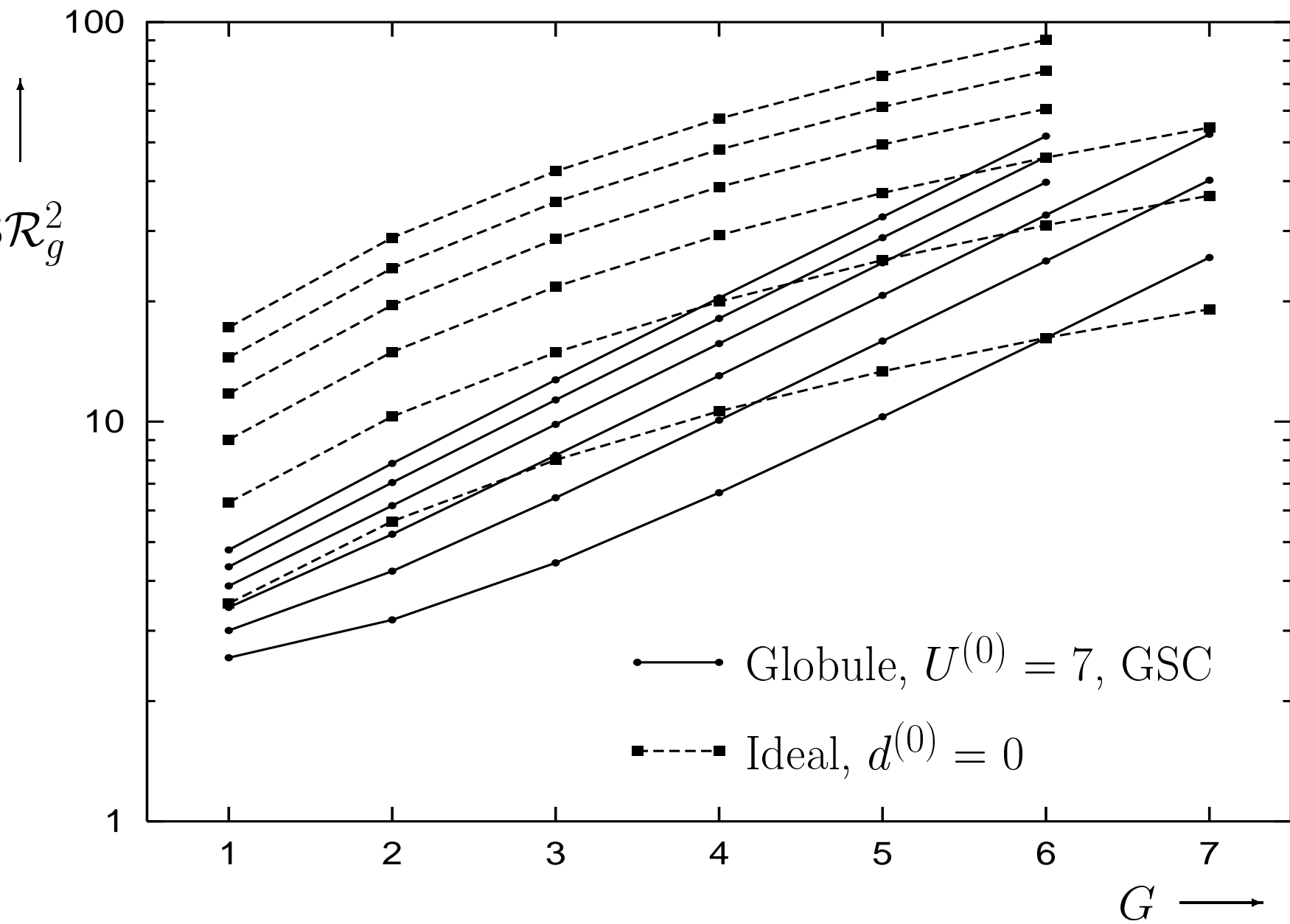


Fig. 13

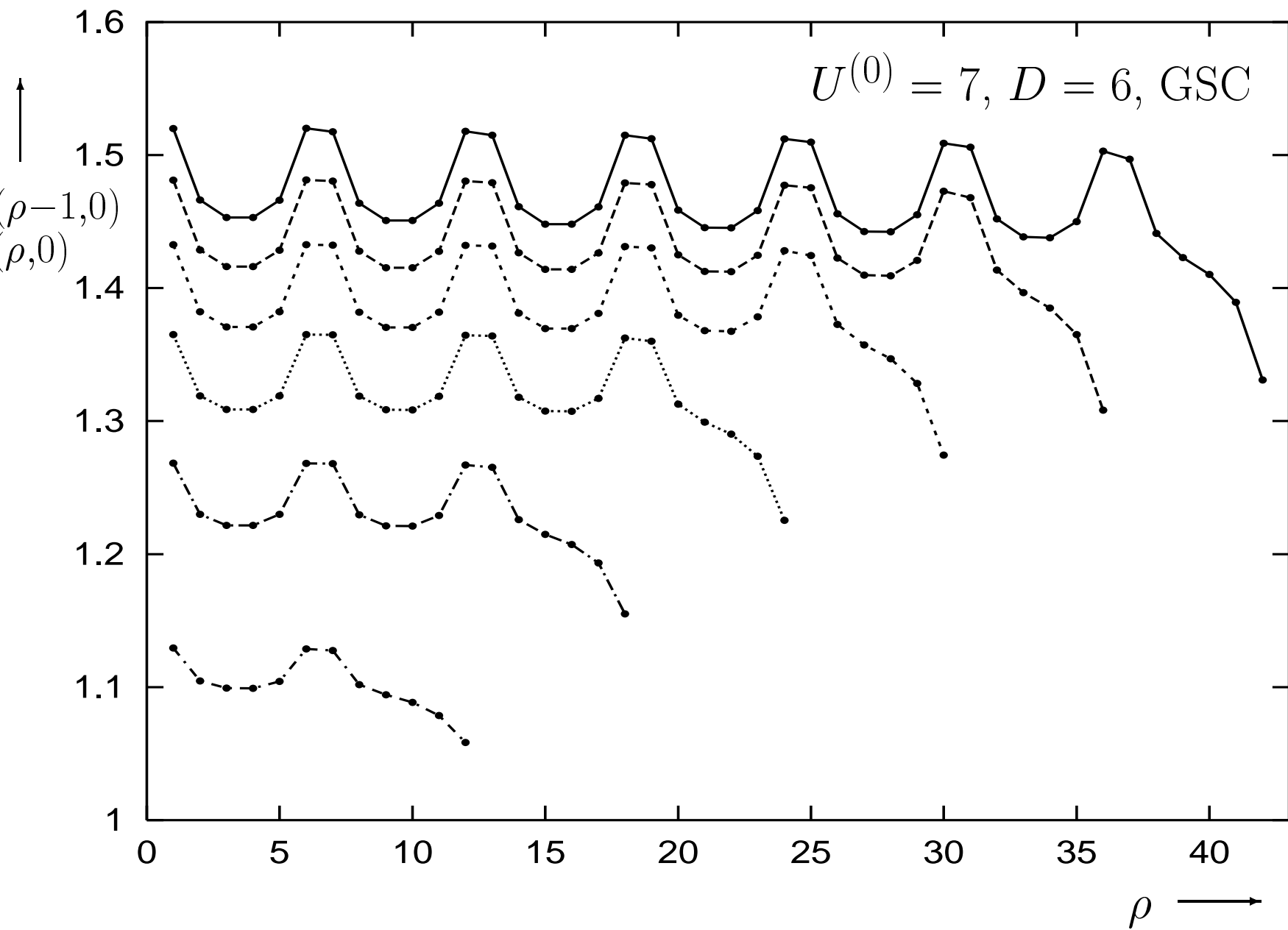


Fig. 14

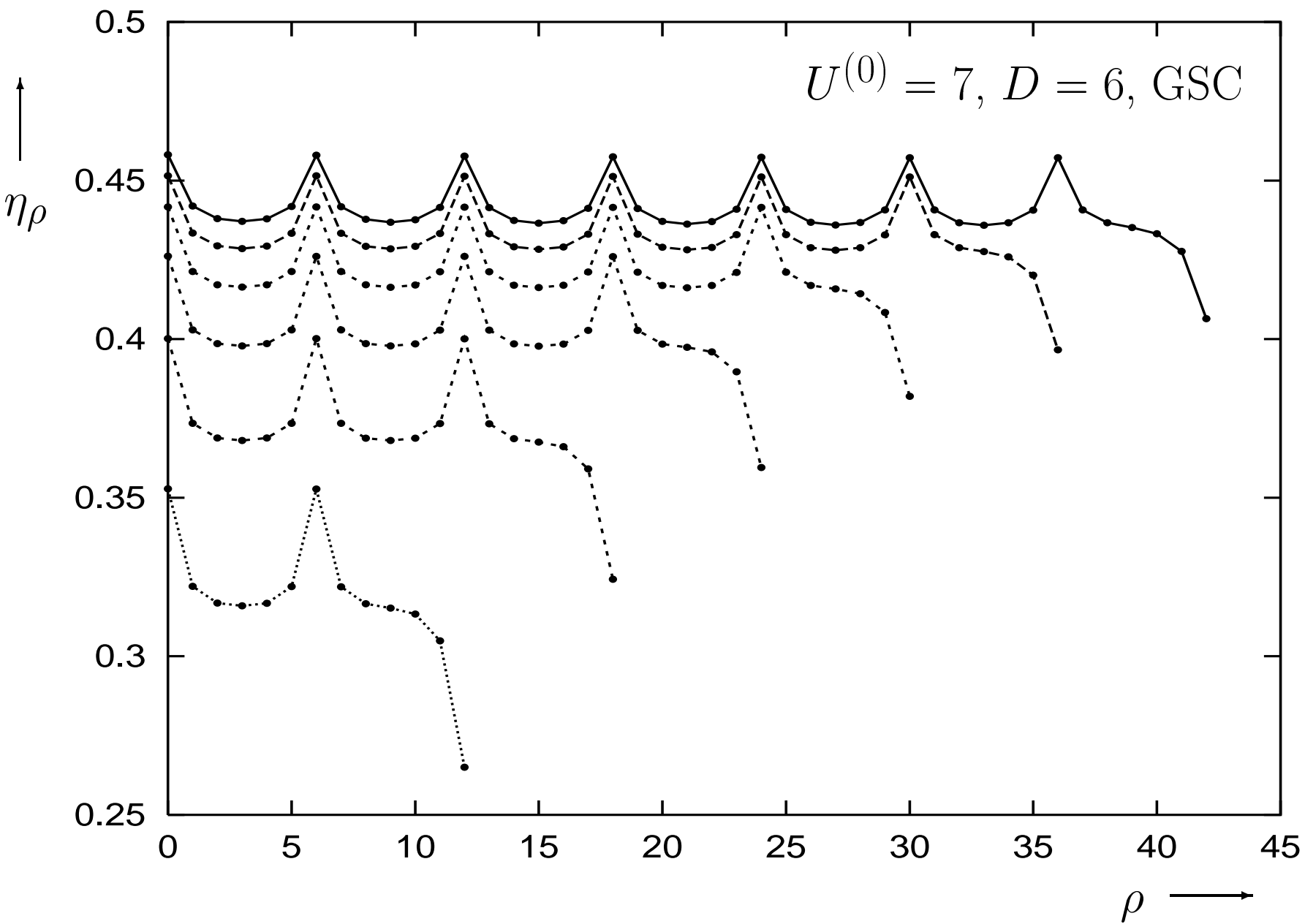


Fig. 15



Fig. 4a

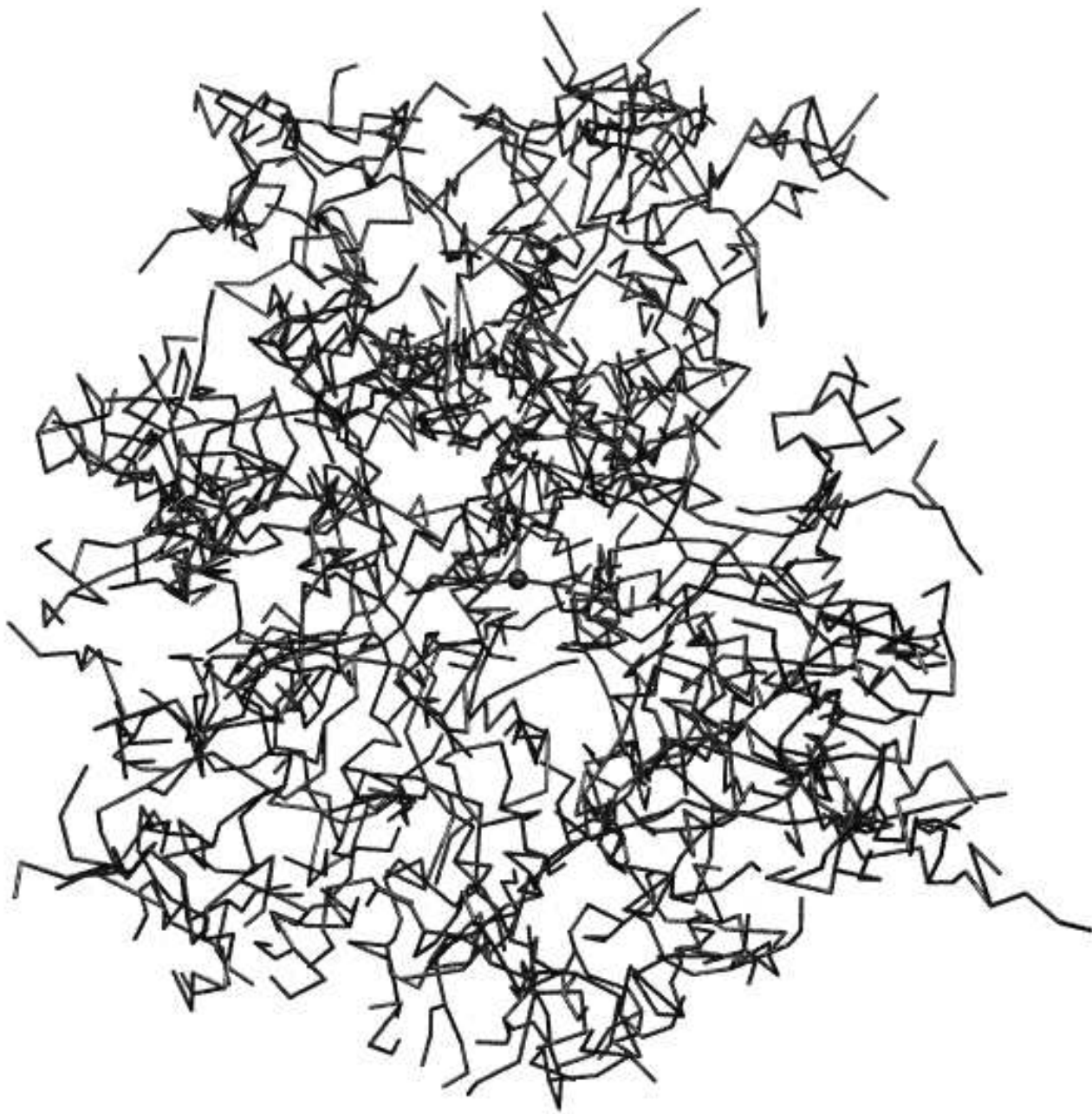


Fig. 4b